Ph.D. Dissertation of Medical Science

Research on the dissemination mechanism of *Mycobacteroides abscessus* through ferroptosis and development of host-directed immune therapy

*Mycobacteroides abscessus*의 ferroptosis를 통한 전파 기전 연구 및 숙주면역기능 강화를 통한 치료법 개발

August 2023

College of Medicine
Seoul National University
Microbiology and Immunology

Hailian Quan

Research on the dissemination mechanism of *Mycobacteroides abscessus* through ferroptosis and development of host-directed immune therapy

Advisor: Prof. Seung Hyeok Seok

Submitting a Ph.D. Dissertation of
Medical Science

April 2023

College of Medicine
Seoul National University
Microbiology and Immunology

Hailian Quan

Confirming the Ph.D. Dissertation written by
Hailian Quan

July 2023

Chair	Bum-Joon Kim	(Seal)
Vice Chair	Seung Hyeok Seok	(Seal)
Examiner	Hang-Rae Kim	(Seal)
Examiner	Sung-Yup Cho	(Seal)
Examiner	Jung Joo Hong	(Seal)

Research on the dissemination mechanism of *Mycobacteroides abscessus* through ferroptosis and development of host-directed immune therapy

지도교수 석 승 혁

이 논문을 의학박사 학위논문으로 제출함
2023년 4월

서울대학교 대학원
의학과 미생물학 전공
전 해 련

전해련의 의학박사 학위논문을 인준함
2023년 7월

위 원 장	김 범 준	(인)
부위원장	석 승 혁	(인)
위 원	김 항 래	(인)
위 원	조 성 엽	(인)
위 원	홍 정 주	(인)

Abstract

Mycobacteroides abscessus (*M. abscessus*) is most common nontuberculous mycobacterial species causing infectious disease in humans. Unfortunately, it is notoriously challenging to treat due to its intrinsic or acquired resistance to first-line anti-TB drugs as well as to most antibiotics commonly used for treatment. The rough morphotype (Ma^{Rg}) of *M. abscessus,* which is distinguished from the smooth morphotype (Ma^{Sm}) by the absence of cell surface glycopeptidolipids (GPLs), is linked to more severe and persistent infection than Ma^{Sm}. However, the precise virulence mechanisms of Ma^{Rg} and its relationship with virulence factors are currently unclear. In this study, the role of ferroptosis in *M. abscessus* infection, specifically in the dissemination of Ma^{Rg}, is investigated. The study suggests that the external cell wall lipid Ma^{Rg}, phosphatidyl-myo-inositol mannoside-Franction 7 (PIM-F7) promotes Ma^{Rg} pathogenicity and propagation by inducing ferroptosis, providing novel insights into the virulence mechanisms of *M. abscessus*. Mechanistically, PIM-F7 is shown to interact with mitochondrial ROS production through TLR2-dependent iron accumulation, which promotes Ma^{Rg} pathogenicity and dissemination by activating lipid

peroxidation and inducing ferroptosis. Overall, these findings shed light on the molecular mechanisms of pathogen-induced ferroptosis and suggest potential therapies targeting iron accumulation-dependent ferroptosis by disrupting *M. abscessus*-host interactions (Chapter 1). This study demonstrates a strong interaction between increasing cellular metabolism and innate macrophage immunity and shows that *Mycobacteroides massiliense* (*M. massiliense*) intracellular replication in macrophages dependents on host pyruvate dehydrogenase kinase (PDK) activity. *M. massiliense* infection triggers a metabolic shift in macrophages, leading to an increase in glycolysis and a decrease in oxidative phosphorylation. However, treatment with the PDK inhibitor dichloroacetate (DCA) reverses this metabolic shift in infected macrophages and restrict intracellular replication.

Mechanistically, DCA activates AMPKα1 by increasing the AMP/ATP ratio, thereby inducing autophagy and limiting bacterial proliferation in phagosomes. These results suggests that pharmacologic inhibition of PDK may represent a promising strategy for host-directed therapy aimed at controlling *M. massiliense* infections (Chapter 2).

Keyword: *Mycobacteroides abscessus*; external cell wall lipid; ferroptosis; dissemination; dichloroacetate; autophagy; host immune defense

Student Number: 2016-31941

General introduction

Mycobacteria extremely exhibit diversity, and recent advancements molecular identification techniques have led to the discover and reclassification of numerous species[1-3]. The bacteria thrive aerobically or under microaerophilic conditions, with their optimal growth occurring between 25 and 50 ℃, depending on the specific species[4]. Out of the approximately 200 identified nontuberculous mycobacteria (NTM) species[2], the majority-around 95%-are found in environmental sources such as soil, air[5], and water[6]. Typically, NTM are found in significant abundance within environmental niches, including soil, natural water sources, and drinking water. This prevalence often results in in frequent interactions between humans and these pathogens[7]. However, only a small number of species within this group have been found to cause disease in in animals and humans. Pathogenic mycobacteria are responsible for various pulmonary and extrapulmonary diseases that can affect any organ in the body. They are typically divided into two main groups: *Mycobacterium tuberculosis* complex that cause tuberculosis, and *Mycobacterium leprae*, the causative agent of leprosy. Other infections resembling those caused by *Mycobacterium*

tuberculosis are attributed to strictly or opportunistically pathogenic mycobacteria referred to as atypical NTM. Numerous NTM species have been identified, some of which act as opportunistic pathogens in both animals and humans. Notably examples include the *Mycobacterium avium* complex and the *Mycobacteroides abscessus* complex (including *Mycobacteroides abscessus* subsp. *abscessus*, *Mycobacteroides abscessus* subsp. boleti, and *Mycobacteroides abscessus* subsp. *massiliense*)[4]. The Runyon classification distinguishes between fast-growing mycobacteria (RGM), which form visible colonies on agar within 7 days, and slow-growing mycobacteria (SGM), which require more than 7 days for colony formation[8, 9]. Most pathogenic mycobacteria belong to the SGM category, implying a potential correlation between growth rate and virulence[4]. In addition, the RGM group primarily consists of saprophytic or non-pathogenic bacteria that do not pose a threat to humans and animals. Lung disease presents the most prevalent clinical manifestation of NTM infection. However, NTM infections display a wide range of phenotypic diversity, giving rise to a broad spectrum of disease that can affect almost nearly any organ[10]. Among the various NTM species, the MAC is the most common causative agent of lung disease exhibits a distinctive feature where

Mycobteroides abscessus complex, a relatively uncommon cause in other countries, emerges as the second most frequent cause in Korea, accounting for approximately 20–30% of cases[11].

Mycobactericidal abscessus has been recognized as the most common cause of RGM infections worldwide, causing skin and soft tissue infections in immunocompetent patients[12, 13], as well as nodular and cavitary granulomas and persistent lung infections in patients with chronic inflammatory lung diseases such as cystic fibrosis (CF), non–CF bronchiectasis, and chronic obstructive pulmonary disease (COPD)[12–16]. *M. abscessus* was first isolated from knee abscesses in 62–year–old patients[17]. Due to its inherent low sensitivity to antibiotics and the presence of both natural and acquired resistance mechanisms, infections caused by *M. abscessus* are notoriously challenging to treat[12, 18, 19]. These infections often exhibit a high rate of treatment failure[20]. On solid agar media, *M. abscessus* exhibits two distinct morphotype: a smooth (Ma^{Sm}) variant, characterized by non–cording but motile and biofilm–forming properties, and a rough (Ma^{Rg}) variant, characterized by cording but non–motile and non–biofilm–forming properties[21]. The primary disparity between these variants lies in the complete absence of surface–associated glycopeptidolipids (GPLs) in the

Ma^{Rg}[22]. Importantly, the emergence of the *Ma*^{Rg} seems to occur exclusively during the course of infection within the host organism, as supported by culture-positive sputum samples from patients[23]. The *Ma*^{Rg} strain of *M. abscessus* is associated with more severe and persistent infections than the *Ma*^{Sm} strain, but the mechanisms underlying its virulence remain unclear.

Macrophages serve as the first line of defense against invading bacterial pathogens and the death of infected macrophages can influence pathogen defense. Once encountered, macrophages recognize bacteria via pathogen-associated molecular patterns (PAMPs) through various pattern recognition receptors (PRRs), which can be found on the cell surface, in vesicles, or the cytoplasm[24]. Surface PRRs not only recognize bacteria but also facilitate their binding, initiating the process of phagocytosis[25]. Specific mycobacterial ligands for these surface PRRs include mannose-capped lipoarabinomannan (manLAM), phosphatidyl-myo-inositol mannoside (PIMs), and trehalose dimycolate (TDM), which are recognized by mannose receptor (MR), DC-SIGN, Mincle, and MCL respectively. In addition to surface receptors, Toll-like receptors (TLRs) also play a crucial role in recognizing mycobacteria. TLRs such as TLR1/2, TLR2/6, TLR4, TLR5, and TLR9 are specific

for lipopeptides, lipopolysaccharides, flagellin, and low-methylated DNA sugar backbone, respectively. Among these, TLR2/6 and TLR9 are particularly important as pivotal PRRs in the context of mycobacterial recognition[25, 26]. *M. abscessus* actively enters macrophages and triggers potent innate immune responses by engaging in a physical and functional interaction between TLR2 and dectin-1. This interaction facilitates internalization of the bacterium and robustly activate immune responses within the macrophages[27].

Cell death in the host is a fundamental mechanism that influences cellular homeostasis, embryonic development, tissue regeneration, and serves as an intrinsic immune defense response to microbial infection. However, bacterial pathogens have devolved diverse strategies to manipulate host cell death and survival pathways in order to facilitate their replication and survival[28]. Apoptosis is a key mechanism employed by human cell to respond to environmental changes. When confronted with microbial infections, cells face a significant challenge, and it is not surprising that the apoptosis machinery has been implicated in numerous infections[29].

Apoptosis could restrict the proliferation of intracellular bacteria[30, 31], whereas high concentrations of *Mycobacterium tuberculosis* (*M. tb*) can lead to necrosis along with the induction of

apoptosis[32]. Recent studies have revealed that the necrotic cell death induced by *M. tb* is ferroptosis[33], which is a cell death mechanism that is dependent on the accumulation of iron. Ferroptosis is a form of regulated necrosis that occurs due to a combination of factors including iron toxicity, lipid peroxidation, and damage the plasma membrane[34]. Iron is an essential ion for the antibacterial effect of macrophages, but it is also necessary for the growth and survival of intracellular bacteria. Hence, a balance in iron levels is crucial to support optimal protection by macrophages during infection. Excessive iron could result in increased oxidative stress that can cause tissue damage[35, 36].

Further investigation has revealed that the external cell wall lipid of Ma^{Rg}, PIM-Fraction 7 (PIM-F7), promotes Ma^{Rg} pathogenicity and dissemination by inducing ferroptosis through TLR2-dependent iron accumulation. PIM-F7 interact with mitochondrial reactive oxygen species (ROS) production, activating lipid peroxidation and inducing ferroptosis. These findings suggest that targeting iron accumulation-dependent ferroptosis by blocking Ma^{Rg} -host interactions could be a potential therapeutic strategy for treating Ma^{Rg} infections (Chapter 1).

Additionally, *Mycobacteroides abscessus* spp. *massiliense* (M.

massiliense), another subspecies of the pathogenic *M. abscessus* complex, is also a significant threat to human health. Studies have shown that *M. massiliense* replication within macrophages is dependent on host pyruvate dehydrogenase kinase (PDK) activity. During *M. massiliense* infection, macrophages undergo a metabolic switch that increases PDK activity and reduces oxidative phosphorylation. However, treatment with the PDK inhibitor dichloroacetate (DCA) can reverse this metabolic switch, thus limiting intracellular bacterial replication.

These findings suggest that pharmacologic inhibition of PDK could be a promising host-directed therapy for controlling *M. massiliense* infection (Chapter 2). In conclusion, these studies have provided valuable insights into the virulence mechanisms of both *M. abscessus* and *M. massiliense* and have identified potential therapeutic targets for managing these highly infectious pathogens. Future research will be required to investigate these mechanisms further and to develop effective treatments for these challenging infections.

Table of contents

Abstract ……i

General Introduction ……iv

Table of contents ……xi

List of figures…… 1

List of abbreviations 3

Chapter 1 5

Introduction..... 6

Materials and methods..... 9

Results 17

Discussion..... 37

Chapter 2 40

Introduction..... 41

Materials and methods..... 44

Results 51

Discussion..... 69

Reference..... 73

국문초록..... 80

List of figures

Chapter 1

Figure 1. Characterization of *M. abscessus* smooth (Ma^{Sm}) and rough (Ma^{Rg}) variant isolates ····· 24

Figure 2. Ma^{Rg} triggers ferroptosis in BMDMs by a mechanism associated with increased intracellular iron, lipid peroxidation, and reduced GPX4 expression ·····25

Figure 3. Ma^{Rg} infection regulates iron export transporters ·····27

Figure 4. Ma^{Rg} external cell wall lipid induces iron accumulation via TLR-2 dependent signaling ·····28

Figure 5. PIMs from Ma^{Rg} extracellular cell wall lipid regulate iron export transporters ·····30

Figure 6. PIMs from Ma^{Rg} induces iron accumulation via TLR2-dependent signaling ·····32

Figure 7. Accumulated iron in Ma^{Rg}-infected macrophages drive mitochondrial ROS production ·····33

Figure 8. Ma^{Rg} induces ferroptosis to promote Ma^{Rg} pathogenicity and dissemination *in vivo*·····35

Chapter 2

Figure 1. DCA decreased glycolysis and intracellular *M. massiliense* in macrophages ·····57

Figure 2. DCA alone had no effect on macrophage viability, bacterial growth ·····59

Figure 3. AMPKa1 deficiency impairs glycolytic and OXPHOS activity in macrophages ·····60

Figure 4. DCA increased phosphorylated AMPKa1 in *M. massiliense*–infected macrophages ·····62

Figure 5. DCA–induced autophagy enhances clearance of intracellular *M. massiliense* in macrophages ····· 64

Figure 6. DCA increased the colocalization of phagosomes and lysosomes against *M. massiliense* infection ····· 66

Figure 7. Schematic depiction of DCA–induced autophagy on *M. massiliense* infection ····· 68

List of abbreviations

NTM: nontuberculous mycobacteria

HDT: host-directed therapy

BMDM: bone marrow-derived macrophage

MOI: multiplicity of infection

DFO: deferoxamine mesylate

TL: total lipid

PIM: phosphatidyl-myo-inositol mannoside

ROS: reactive oxygen species

LPO: lipid peroxidation

TLR2: Toll-like receptor 2

PDK: pyruvate dehydrogenase kinase

PDH: pyruvate dehydrogenase

DCA: dichloroacetate

PMA: phorbol 12-myristate 13-acetate

MOI: multiplicity of infection

CFU: colony-forming units

OXPHOS: oxidative phosphorylation

ECAR: extracellular acidification rate

OCR: oxygen consumption rate

AMP: adenosine monophosphate

ATP: adenosine triphosphate

Chapter 1

External cell wall lipid in *Mycobacteroides abscessus* induces ferroptosis and dissemination

Introduction

Mycobacteroides abscessus (*M. abscessus*) is increasingly recognized as a human pathogen due to its ability to cause a wide range of clinical manifestations, including mucous skin infections and disseminated or chronic lung disease[4]. This species is notoriously one of the most drug-resistant mycobacteria, characterized by a wide range of intrinsic and acquired drug resistance mechanisms that make it resistant to almost all anti-TB drugs and various classes of antibiotics. As a result, *M. abscessus* is responsible for complex, prolonged treatment, and high rates of treatment failure. Clinical isolates of *M. abscessus* have two morphotypes: smooth (Ma^{Sm}) and rough (Ma^{Rg})[22, 37]. Epidemiological studies have associated Ma^{Rg} with a rapid decline in lung function and an acute respiratory syndrome that can persist for years in the host[23, 38, 39]. Ma^{Sm} and Ma^{Rg} have distinct differences in inducing immune cell death and inflammation upon infection. Ma^{Rg} induces more apoptosis than Ma^{Sm}, but it also induces more necrotic cell death[40, 41]. This suggests that Ma^{Rg} induces other types of cell death besides apoptosis. However, our knowledge of the effects or interactions between Ma^{Rg}-induced cell death and pathophysiological properties is

incomplete.

Host cell death is a fundamental process that shapes cellular homeostasis, embryonic development, and tissue regeneration, as well as an intrinsic immune defense mechanism in response to microbial infection. However, bacterial pathogens have evolved various strategies to manipulate host cell death and survival pathways to replicate and survive[28]. The glycopeptidolipids (GPLs) of *Ma*^{Sm} inhibits apoptosis by regulating the mitochondrial membrane potential[41], while *Ma*^{Rg} activates the inflammasome by regulating mitochondrial oxidative stress[42]. Iron and reactive oxygen species (ROS) are increasingly recognized as important initiators and mediators of cell death in various organisms and pathological situations[43]. Simultaneous accumulation of iron and ROS production induces ferroptosis, a type of cell death. However, there is a lack of research on iron-dependent cell death and iron regulation during *M. abscessus* infection.

The homeostasis of iron in cells can be regulated by membrane transport channels and stores. Among them, iron export channels include ferroportin and lipocalin-2. TLR2 inhibits the expression and translocation of ferroportin, regulating the accumulation of intracellular iron, and *Ma*^{Rg} interacts with TLR2. Therefore, it is likely

that *Ma*^{Rg} regulates ferroprotin by modulating TLR2 signaling. In addition, lipocalin-2 has been linked to TLR2[44]. One explanation for the greater toxicity of *Ma*^{Rg} is that the loss of GPLs masks cell wall inflammatory lipoproteins[45] or PIM[46], which are known agonists of TLR2[47].

In this study, I evaluated the role of iron accumulation in cell death induced by *Ma*^{Rg} infection in BMDMs. I found that *Ma*^{Rg} infection induces ferroptosis, which is associated with downregulation of ferroprotin expression, upregulation of hepcidin and lipocalin2 expression, and the generation of mitochondrial ROS. Mechanistically, PIM-F7 in the *Ma*^{Rg} cell wall promotes the activation of TLR2, which inhibits the expression of ferroportin, promotes the expression of hepcidin and lipocalin2, accumulates iron, and activates the production of mitochondrial ROS to induce ferroptosis. I found that treatment with a ferroptosis inhibitor could reduce the lung lesions developed in *Ma*^{Rg}-infected mice. These results indicate that cell death is regulated by the PIM-F7-TLR2-iron efflux axis in *Ma*^{Rg} infection, providing insights into the pathogenesis and treatment of *Ma*^{Rg} in particular.

Materials and methods

Bone Marrow-Derived Macrophages (BMDMs)

Bone marrow-derived macrophages (BMDMs) were prepared from the femoral, tibial, and pelvic bone marrow of both male and female mice. BMDMs were differentiated by culturing bone marrow cells on non-tissue culture treated dishes for 5 days in RPMI containing 10% FBS, 1% penicillin/streptomycin, 1% L-glutamine (Gibco), and 20% L929 cell-conditioned medium at 37℃ with 5% CO_2. Matured BMDMs were scraped form dishes, reseeded at a density of 2.5 x10^5 cells per well in a 24-well plate in antibiotic-free complete medium, and rested for 2 days.

Bacterial culture

The *Ma*^{Sm} has a smooth colony phenotype, while *Ma*^{Rg} have a rough phenotype. Briefly, *Ma*^{Rg} is a rough isolate from spontaneously dissociated from *Mg*^{Sm} when subcultured in our lab. *M. abscessus* was cultured in Middlebrook 7H9 medium (BD Biosciences) supplemented with 10% ADC, 0.2% glycerol, and 0.05% Tween 80 (Sigma-Aldrich). The cultured bacteria were collected via centrifugation. The collected mycobacteria were stored at −80℃ until use. To prepare single cells

of *M. abscessus*, cultured bacteria were homogenized with a 23-gauge syringe needle for 10 min after a soft-spin centrifugation to exclude bacterial clumping. The number of viable bacteria in the stored bacterial vials was counted on 7H11 agar (Sigma-Aldrich).

In vitro macrophage infection and stimulation

On the day of infection, BMDMs were replenished with relevant complete media formulations described above (without antibiotics). Cells were exposed to *M. abscessus* at the indicated multiplicity of infection (MOI) for 2 hours, washed two times with 1x PBS, and then cultured in fresh Opti-MEM media for 1 day. In some experiments, Z-VAD (10 μM)(Santa Cruz), Nec-1 (10 μM), Fer-1 (10 μM), Lip-1 (1 μM), or DFO (200 μM) (Sigma-Aldrich) was added to the cultures 1hour before infection and then maintained in the same media for the entire experiment. BMDMs cells were pretreat with 40 μg/㎖ of lipid for 2 hour and then infected with Ma^{Sm}, or BMDM cells were direct treated with lipid for 24 hours.

Measurement of cell death

Necrotic cell death was evaluated by staining cells with either Live/Dead fixable aqua dead cell stain kit, 7-AAD (Invitrogen), or

Annexin V (BioLegend) according to the manufacturer's protocol. Briefly, uninfected and infected cells were first stained with specific antibodies for CD11b (eBioscience) at room temperature for 15 min and then washed with 1× PBS following centrifugation at 2,000 rpm for 5 min. Live/Dead staining solution (1:750 diluted in 1× PBS) was added to the macrophage cultures and incubated at room temperature for 15 min in the dark. Then cells were washed with 1× PBS twice and analyzed by flow cytometry. Cellular necrosis was also assessed by measuring the release of LDH in the supernatants from macrophage cultures with CytoTox 96 nonradioactive cytotoxicity assay (Promega) according to the manufacturer's instructions. In some experiments, annexin V staining was performed to evaluate apoptotic versus necrotic cell death in *M. abscessus*–infected macrophage cultures. Briefly, BMDMs were stained with Annexin V diluted in annexin–binding buffer (BD Biosciences) for 20 min, washed with 1× PBS, and then counterstained with anti–CD11b and Live/Dead fixable aqua dead cell stain kit or 7–AAD. The samples were then analyzed by flow cytometry.

Western blot analysis

Total cell lysates were prepared by harvesting the cells in sample

buffer (Biosesang, Gyeonggi-do, Korea) with protease and phosphatase inhibitors (GenDEPOT, Katy, TX, USA), sonicated for 40 s, and heated to 99℃ for 5 min. Proteins were resolved on 12% polyacrylamide gels and transferred to polyvinylidene difluoride membranes (Merck Millipore, Burlington, MA, USA). Anti-Glutathione Peroxidase 4 (Gpx4) (Abcam) and anti-β-actin (Santa Cruz) were used to investigate protein expression.

Metabolism analysis

To measure mitochondrial mass and membrane potential, cells were resuspended in medium (RPMI1640) containing Mitotracker (5 nM) and/or Tetramethylrhodamine, methyl ester (TMRM) (25 nM) (Invitrogen). After incubation at 37℃ for 30 minutes, cells were washed twice with 1xPBS followed by standard surface staining and flow cytometric analysis. To measure the production of mitochondrial ROS, cells were stained with MitoSox (5 mM) (Invitrogen) in HBSS at 37℃ for 30 minutes, followed washed with HBSS twice, standard surface staining and analysis on a flow cytometer.

RNA extraction and quantitative real-time PCR analysis

Total RNA was extracted using the TRIzol reagent (Invitrogen,

Waltham, MA, USA) according to the manufacturer's instructions. Complementary DNA was synthesized from total RNA by reverse transcription, and the amount of mRNA was determined by real-time PCR analysis using SYBR Green qPCR PreMix (Enzynomics, Daejeon, South Korea) on an ABI real-time PCR 7500 machine (Applied Biosystems, Waltham, MA, USA). Samples were normalized to the β-actin levels. PCRs were performed using primers for *Tfrc* (forward, 5′-GTA GTC TCC ACG AGC GGA ATA-3′; reverse, 5′-CCC ATG ACG TTG AAT TGA ACC T-3′), *Trf* (forward, 5′- ATA CCG ATG CTA TGA CCT TGG AT-3′; reverse, 5′- CAG GAC TTC TTG CCT TCG AG-3′), *Hamp* (forward, 5′- CAT GAT GGC ACT CAG CAC TC-3′; reverse, 5′- GGT CAG GAT GTG GCT CTA GG-3′), *Slc40a1* (forward, 5′- TGG ATG GGT CCT TAC TGT CTG CTA C-3′; reverse, 5′- TGC TAA TCT GCT CCT GTT TTC TCC-3′), *Lcn2* (forward, 5′- CCA TCT ATG AGC TAC AAG AGA ACA AT-3′; reverse, 5′-TCT GAT CCA GTA GCG ACA GC-3′), and *Gpx4* (forward, 5′-GCA ACC AGT TTG GGA GGC AGG AG-3′; reverse, 5′-CCT CCA TGG GAC CAT AGC GCT TC-3′).

Lipid purification

Ma^{Rg} from a 100 ㎖ culture was harvested at 4,000 rpm and the

supernatant was removed. The weight of wet cells was determined, and for each gram of bacteria, one ㎖ lysis buffer ($CHCl_3$/CH_3OH (2:1)) was added. The cells were then sonicated at 56℃ for 40 min (20 min each time) and incubated at 4℃ overnight. The lysates were centrifugation at 4,000 rpm to remove unbroken cells and filtered using a PTFE filter with Millipore 0.22㎛. The lipid was air-dried and stored at -20℃ until use. Lipid (PIM) solation was performed using LC-MS/MS.

Immunofluorescence microscopy

To perform immunofluorescence staining, Ma^{Rg}-infected cells were fixed with 4% paraformaldehyde (PFA) for 15 min, and permeabilized with 0.1% Triton X-100 for 5 min and blocked in 1% BSA/PBS for 1 hour at room temperature. The samples were subsequently incubated with rabbit anti-SLC40A1 (NOVUS) antibody (diluted 1:50-1:100 in antibody solution) at -4℃ overnight. They were then washed and incubated with Alexa 594-conjugated anti-rabbit IgG (Thermo Fisher) at 1:200 dilution for 90 min. Lastly, the slides were examined using fluorescence microscopy.

Microinjection of Mycobacteria into zebrafish embryo

Mycobacterial strains stained with DiI were resuspended in PBS. Bacterial suspensions were homogenized through a 26-gauge needle and sonicated three times for 10 seconds each to disperse the bacteria. Any remaining clumps were allowed to settle for 5-10 min. The supernatants were resuspended at an OD_{600} of 1 in PBS with phenol red. Infection was carried out by microinjection of 2-3 nL of bacterial suspensions, containing 150-300 bacteria, into the yolk sac of dechorionated and anesthetized embryos at 30 hpf. To follow infection kinetics, infected embryos were transferred into individual wells and incubated at 28.5℃. The inoculum size was checked a posteriori by injection in sterile PBS and plating on 7H11 agar containing 10% (vol/vol) OADC. Survival curves were established by counting dead embryos (no heartbeat) every day, for up to 10 days.

Animal infection.

Seven to eight-week-old, specific-pathogen-free female SCID/beige mice (NOD.CB17-*Prkdc*$^{scid/scid}$/Rj) were infected intranasally with 30 ㎕ containing 1 x10^6 CFU of *M. abscessus*. After 28 days of infection, mice were sacrificed, and organs were homogenized in 1xPBS. Serial dilutions were plated on nutrient 7H11 agar for 3-4 days 37℃, and CFU were enumerated. All experimental protocols

were approved by the Animal Care and Use Committee of Seoul National University (accession number SNU-210412-2-2).

In vivo determination of lipid peroxidation in lungs

Briefly, lungs were homogenized in 1xPBS and centrifuged at 12,000 rpm at 4℃ for 10 min to remove tissue matrix and cell debris. Supernatants were harvested, filter sterilized, and stored at −80℃. Lipid peroxidation was measured by using the TBARS assay kit (Cayman Chemical) according to the manufacturer's instruction.

Statistical analyses

All statistical analyses were performed using GraphPad Prism version 8.0 (GraphPad) and are shown as mean ± standard error of the mean.

Results

Ma^{Rg} causes a significantly higher level of macrophage cell death

To elucidate the relationship between cell death and *M. abscessus* toxicity, I compared the cell death response of macrophages infected with *Ma*^{Sm} or *Ma*^{Rg}. First, I compared the cell growth and aggregation of *Ma*^{Sm} and *Ma*^{Rg}. I obtained the same growth rate of *Ma*^{Rg} as *Ma*^{Sm} by spontaneous transfection of *Ma*^{Sm} (Fig. 1A). However, I found that aggregation was higher in *Ma*^{Rg} than in *Ma*^{Sm}, which is consistent with previous studies (Fig. 1B). I also found that aggregation was less in the presence of glycerol and Tween80. Next, I infected BMDM cells with *M. abscessus* at a multiplicity of infection (MOI) of 5. At 48 hours, I noticed that there were dead cells (Fig. 1C). In particular, the cells infected with *Ma*^{Rg} were crushed to death. I ran an LDH release assay and found that there was dramatically more death in *Ma*^{Rg} (Fig. 1D).

Macrophage necrotic cell death induced by *Ma*^{Rg} is ferroptosis

Previous studies have shown that *Ma*^{Rg} induces more apoptosis[41], but late in the infection, the appearance of cell death shows necrotic cell death features (Fig. 2A). Infected cells exhibit heightened

secretion of ROS. ROS play a pivotal role in regulating various forms of cell death, including apoptosis, necrosis, and ferroptosis[48]. I hypothesized that it was ferroptosis and first checked the accumulation of iron by staining for FeRhoNox-1. Increased accumulation of iron in *Ma*^{Rg} -infected macrophages was confirmed by confocal imaging and quantified using FACS 12 hours post-infection (Fig 2B and 2C). LPO was monitored by staining with BODIPY C-11, and the fluorescence intensity was observed at time intervals of 12 to 48 hours, with confocal images were taken at 24 hours. I found that LPO was significantly higher in macrophages infected with *Ma*^{Rg} (Fig. 2D and 2E). I also examined the expression of GPX4, a key enzyme in the regulation of ferroptosis, by Western blot (Fig. 2F) and FACS (Fig. 2G) and found that its expression was reduced in *Ma*^{Rg}-infected macrophages 6 hours post-infection. These results suggest that the necrotic cell death of *Ma*^{Rg}-infected macrophages is ferroptosis.

Iron accumulation in *Ma*^{Rg}-infected macrophages is regulated by the iron export channels

Ferroptosis is characterized by the accumulation of iron. To determine how iron accumulates in *Ma*^{Rg}-infected macrophages, I

checked the expression of mRNAs of iron transporters after infection. I investigated the expression of iron import transporters *Trf*, *Tfrc*, and *Dmt1* and export transporters *Lcn2*, *Hamp*, and *Slc40a1* at 6 hours post-infection. I did not observe statistical significance in the expression of the import channels *Trf*, *Tfrc*, and *Dmt1*, but the expression of the export channel *Slc40a1* was significantly decreased in Ma^{Rg}, while *Hamp*, which acts as a gate for ferroportin (SLC40A1), was increased (Fig. 3A). I also observed that the expression of *Lcn2*, which helps iron exit, was significantly increased in Ma^{Rg}-infected macrophages (Fig. 3A). Based on the previous findings that lipocalin-2 (LCN2) is used to move iron from macrophages to neighboring cells, I indirectly proved that LCN2 was used to facilitate the dissemination of ferroptosis. Furthermore, I stained the expression of SLC40A1 and observed it by confocal fluorescence images and found that its expression was decreased in Ma^{Rg}-infected macrophages (Fig. 3B).

PIM-F7 in external cell wall lipids of Ma^{Rg} accumulates intracellular iron

The biggest difference between Ma^{Rg} and Ma^{Sm} is that Ma^{Sm} masks the signal of PIMs below with GPLs on the surface[46]. I

hypothesized that the external cell wall lipids of *Ma*^{Rg} transmit signaling that leads to iron accumulation, so I isolated all the external cell wall lipids of *Ma*^{Rg} and obtained eight fractions by LC-MS/MS (Fig. 5A). First, I treated BMDM cells with total lipids (TL) directly or by coating with beads (TL Beads), and all both of TL and TL Beads increased the accumulation of iron (Fig. 4A). Among them, I confirmed that iron accumulated in the vehicle when coating with beads, so I chose the direct treatment method for further experiments. Then, I investigated the mRNA levels of *Lcn2*, *Hamp*, and *Slc40a1* at 6 hours post-treatment with TL. Previous studies have shown that GPL-masked PIMs interact with TLR2 to induce inflammatory responses. Therefore, I investigated the accumulation of iron after treatment with TLR2 antibody or at TLR2$^{-/-}$ BMDM cells and found that the accumulation of iron was inhibited in a TLR2-dependent manner (Fig. 4C and 4D). I wondered if pretreatment with TL before infection would regulate cell death. As a result, more cell death was observed in the TL-treated group (Fig. 4E). Next, I wanted to know which of the fractions was responsible for the accumulation of iron, so I first performed PCR for genes related to the iron export channels. I found that PIM-F7 and PIM-F8 increased *Lcn2* and *Hamp* and decreased *Slc40a1* in the same trend as TL (Fig.

5B). Among them, I chose PIM-F7 based on its greater increase in the expression of *Lcn2* and hypothesized that it was the factor inducing the accumulation of iron. I treated cell with PIM-F7 and analyzed whether iron accumulation increased in a TLR2-dependent manner using FACS (Fig. 6A and 6B). I found that 24 hours after PIM-F7 treatment, iron accumulation was increased in wild type, but not in TLR2$^{-/-}$ BMDM cells. From this, I conclude that PIM-F7, an external cell wall lipid of *Ma*^{Rg}, induces ferroptosis by inducing iron accumulation in a TLR2-dependent manner. In the group pretreated with PIM-F7, as in the group treated with TL, more cell death was observed (Fig. 6B).

Accumulated iron regulates mitochondrial ROS production and ferroptosis

It is well known that increased production of ROS can cause ferroptosis. Mitochondria play a central role in the response to apoptotic stimuli and are a major source of ROS in cells. I investigated whether mitochondrial ROS were involved in the accumulated iron-mediated ferroptosis in BMDM cells. First, I confirmed by confocal imaging that mitochondrial ROS and quantified by FACS, mitochondrial ROS was increased more in the *Ma*^{Rg}-infected group in

infected macrophages (Fig. 7A and 7B). Then, I performed FACS fractionation and found that the destruction of $\Delta\Psi$m was also more (Fig 7C and 7D). Mitochondrial ROS are mainly generated in the electroporation chain, and iron is a requirement for this process[49, 50]. Therefore, I examined the production of mitochondrial ROS and found that it was inhibited by iron chelation (Fig. 7E). I also found that LPO activation (Fig. 7F) and cell death (Fig. 7G) was inhibited by iron chelation. From these, I confirmed that iron accumulated by *Ma*^{Rg} induces the production of mitochondrial ROS and ferroptosis.

Ma^{Rg} promotes pathogenicity and dissemination through ferroptosis

It is widely recognized that *Ma*^{Rg} exhibits higher virulent than *Ma*^{Sm} in *M. abscessus*–infected mice, as evidenced by bacterial growth in the lungs[51], and at the cellular level by its ability to incude cell death and escape from macrophages. To investigate whether the dissemination of *Ma*^{Rg} in vivo is facilitated by ferroptosis, I evaluated its pathogenicity and dissemination in zebrafish and mice. My findings in zebrafish indicate that infection with *Ma*^{Rg} leads to higher mortality, increased bacterial growth by day 7, and more caudal migration in yolk sac–infected larvae, which is consistent with previous studies. (Fig. 8A–C). In mice, I intranasally infected them and found that the

number of bacteria in the lungs did not differ significantly between *Ma*^{Sm} and *Ma*^{Rg}, but *Ma*^{Rg} had higher bacterial burdens in the spleen and liver organs (Fig. 8D). Furthermore, I observed a higher increase in MDA levels, a byproduct of lipid peroxidation, in the lungs of *Ma*^{Rg}–infected mice (Fig. 8E). Collectively, these data suggest that *Ma*^{Rg} may contribute to the dissemination of the bacteria through the induction of ferroptosis.

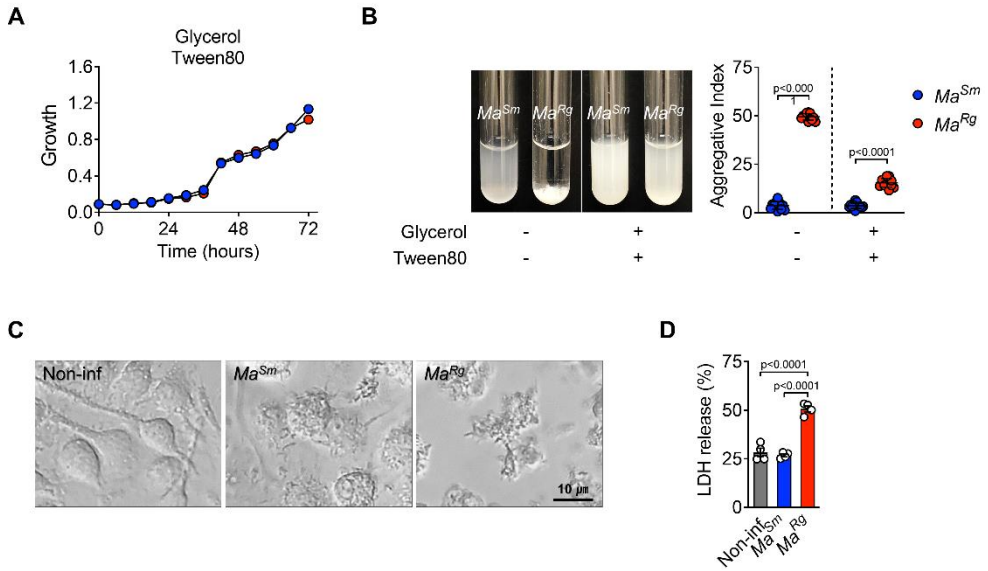

Figure 1. Characterization of *M. abscessus* smooth (*Ma*^{Sm}) and rough (*Ma*^{Rg}) variant isolates. (A) Isolated *Ma*^{Rg} and *Ma*^{Sm} colonies were grown in 7H9 broth. Growth was similar for the two variants in 7H9 broth with glycerol and Tween 80. (B) When cultures were removed from shaking after 15 min, *Ma*^{Sm} remained suspended, but *Ma*^{Rg} rapidly settled out in the absence of glycerol and Tween 80. Aggregation index was significantly reduced with glycerol and Tween 80. (C) BMDM cells were infected with *Ma*^{Rg} or *Ma*^{Sm} (MOI=5) for 48 h. (D) Cell death was analyzed using LDH release assay kit. In panels B, p-values are indicated (two-way ANOVA). In panel D, p values are indicated (one-way ANOVA). Error bars represent the mean and standard error of the mean (SEM); n=3

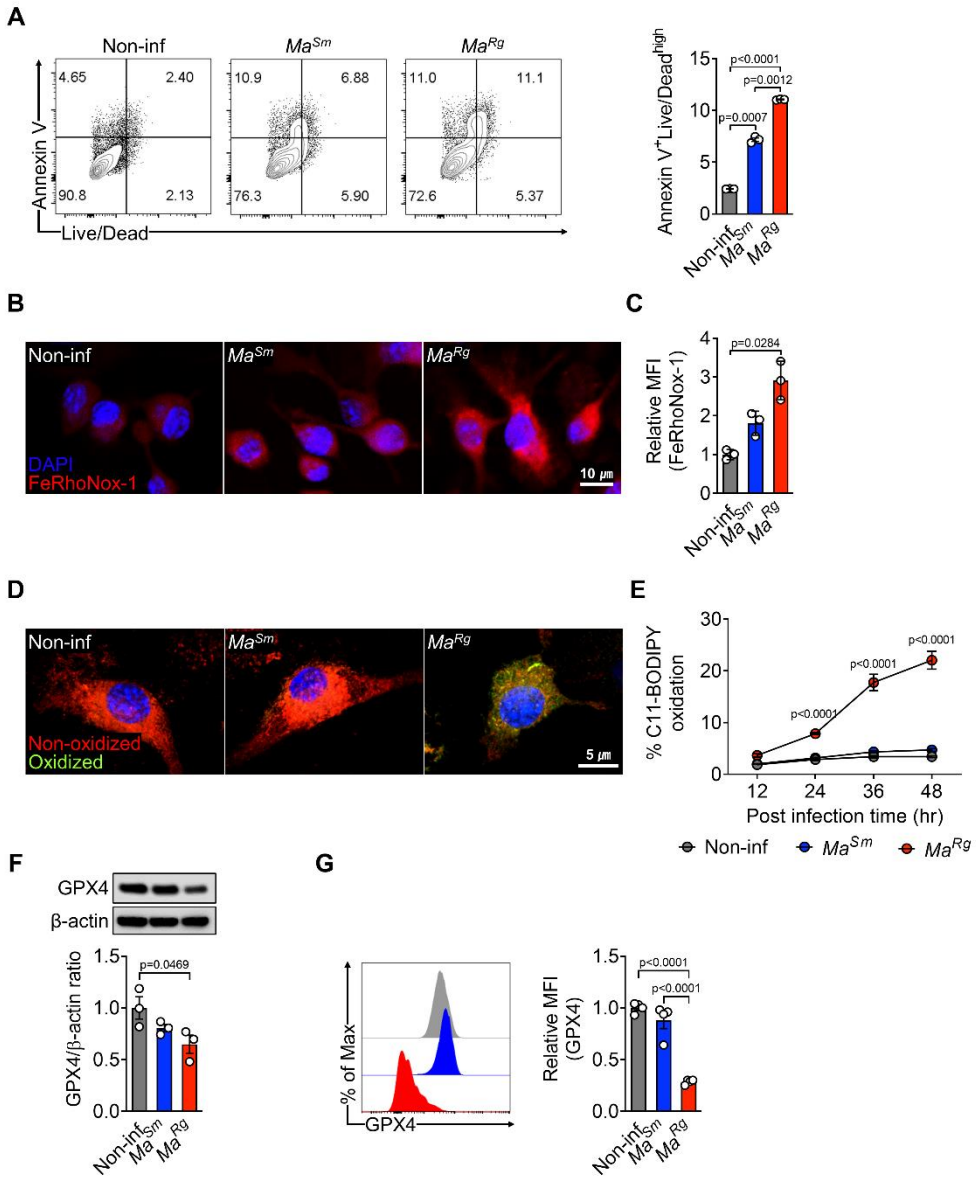

Figure 2. *Ma*^{Rg} triggers ferroptosis in BMDMs by a mechanism associated with increased intracellular iron, lipid peroxidation, and reduced GPX4 expression. (A) BMDM cells were infected with *M. abscessus* (MOI=5) for 2 h, then cells were washed, and the medium was replaced for 24 h. Cell death was measured by Annexiv V and

Live/Dead fixable aqua staining using FACS analysis. (B) BMDM cells infected with *M. abscessus* (MOI=5) for 2 h, then cells were washed, and the medium was replaced for 12 h. Intracellular iron was stained with FeRhoNox-1 and subjected to fluorescence microscopy. Scale bars, 10 ㎛. (C) Intracellular iron was quantified under FACS analysis. (D) To investigate the lipid peroxidation, BMDM cells were infected with *M. abscessus* (MOI=5) for 2h, then cells were washed, and the medium was replaced for 24 h. (E) Fluorescence intensity was measured over time up to 48 h. (F) Intracellular GPX4 protein levels detected by Western blotting and quantitated using ImageJ (G) GPX4 expression assessed by MFI of GPX4 staining in CD11b+/live cells by flow cytometry. All data are representative of three independent experiments. Statistical significance is indicated by p-values (one-way ANOVA), and error bars represent the mean and standard error of the mean (SEM). n=3-4.

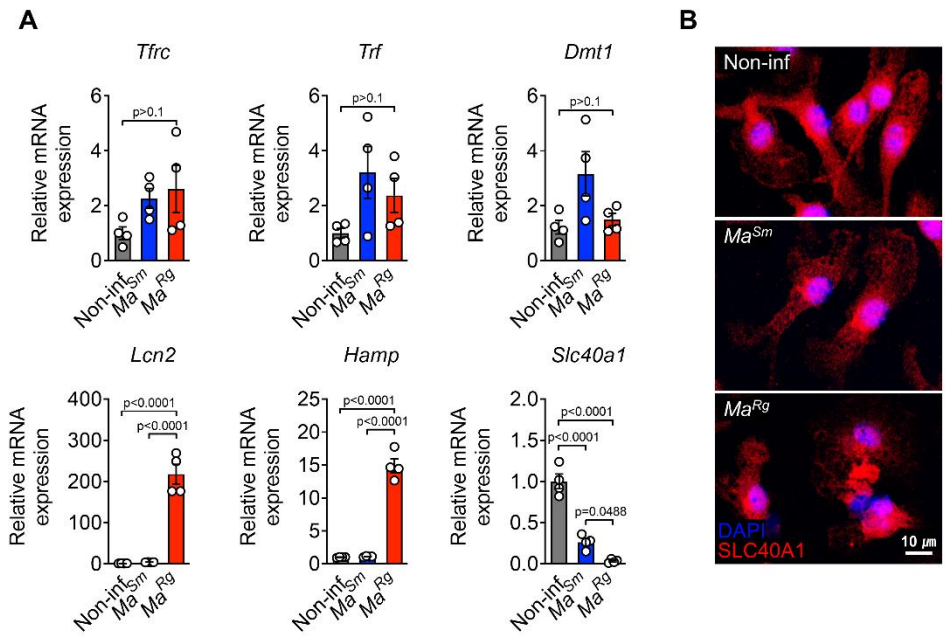

Figure 3. *Ma*^{Rg} infection regulates iron export transporters. (A) BMDM cells were lysed, total RNAs were extracted, and the expression of *Trf, Tfrc, Dmt1, Lcn2, Hamp*, and *Slc40a1* at mRNA level was determined by qRT-PCR. Cells were infected with *M. massiliense* (MOI=5) for 2 h, and then washed; the medium was replaced for 12 h. (B) BMDM cells infected with *M. abscessus* (MOI=5) for 2 h then cells were washed, and the medium was replaced for 24 h. Then intracellular iron was staining with SLC40A1 antibody and subjected to fluorescence microscopy. All data are representative of three independent experiments. Statistical significance is indicated by p-values (one-way ANOVA), and error bars represent the mean and standard error of the mean (SEM). *n*=3-4.

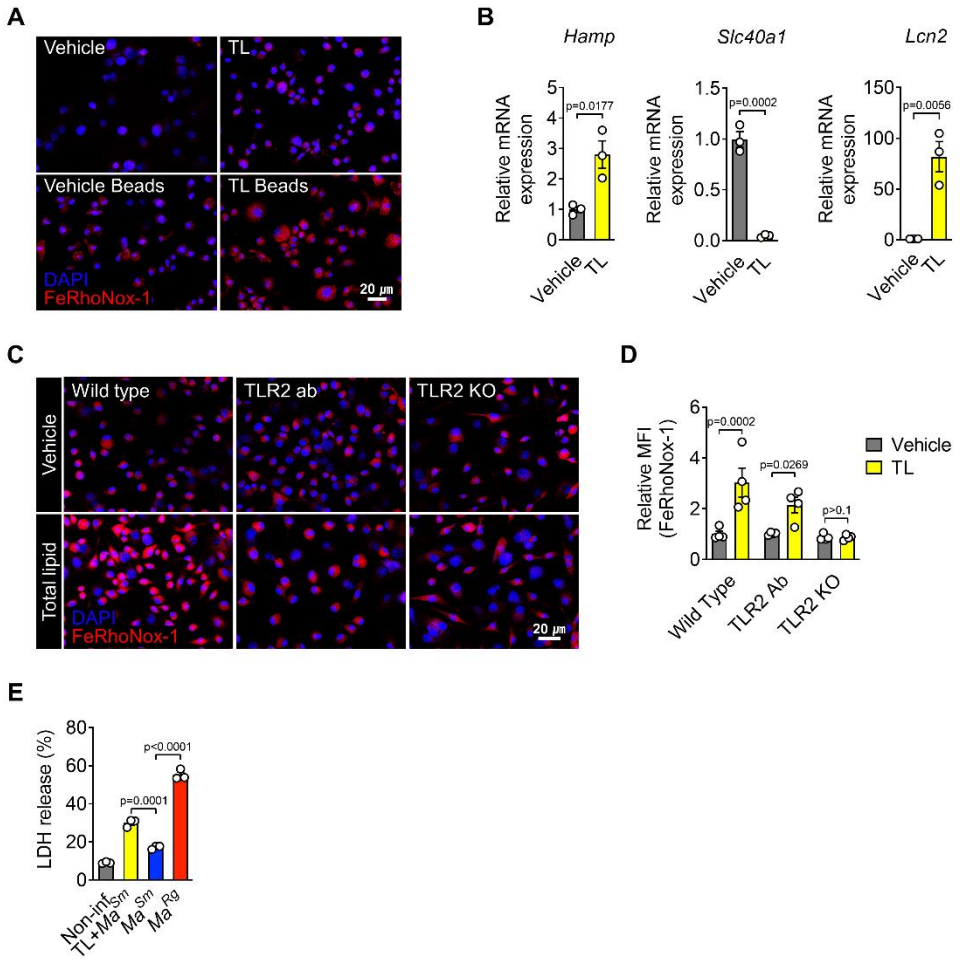

Figure 4. *Ma*^{Rg} external cell wall lipid induces iron accumulation via TLR2-dependent signaling. (A) BMDM cells were treat total lipid directly or TL-coated beads for 24 h. Then cells were stained with FeRhoNox-1 and subjected to fluorescence microscopy. (B) BMDM cells were lysed, total RNAs were extracted, and the expression of *Lcn2, Hamp*, and *Slc40a1* at mRNA level was determined by qRT-PCR. Cells were treated with TL (40 ㎍/㎖) for 12 h. (C) Wild type and TLR2$^{-/-}$ BMDM cells were treat TL directly for 24 h, then cells

were stained with FeRhoNox-1 and subjected to fluorescence microscopy. (D) Intracellular iron was quantified under FACS analysis. (E) BMDM cells infected with *M. abscessus* (MOI=5) for 2h. Then, cells were washed, and the medium was replaced for 48 h. Cell death was measured by LDH release assay. All data are representative of three independent experiments. In panels A, p-values are indicated (unpaired t-test). In panel D, p-values are indicated (two-way ANOVA). In panel E, p-values are indicated (one-way ANOVA) Error bars represent the mean and standard error of the mean (SEM). n=3.

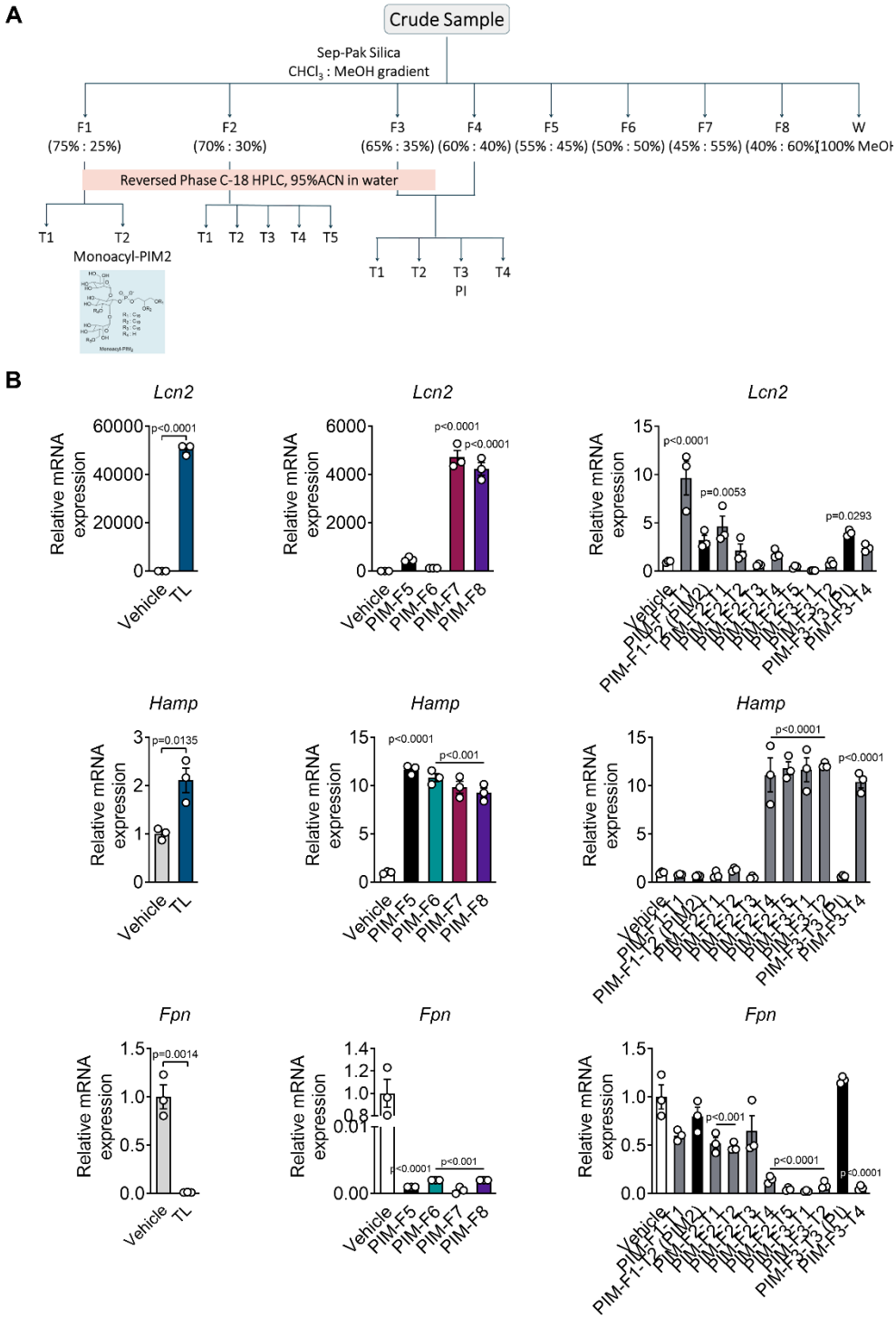

Figure 5. PIMs from *Ma*^{Rg} extracellular cell wall lipid regulate iron export transporters. (A) Scheme for LC-MS/MS. (B) BMDM cells

were lysed, total RNAs were extracted, and the expression of *Lcn2, Hamp*, and *Slc40a1* at mRNA level was determined by qRT-PCR. Cells were treated with PIMs (40 ㎍/㎖) for 12 h. All data are representative of three independent experiments. Statistical significance is indicated by p-values (unpaired t-test, one-way ANOVA), and error bars represent the mean and standard error of the mean (SEM). n=3.

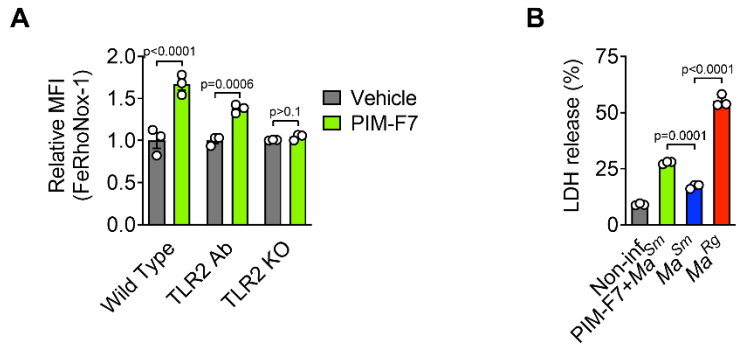

Figure 6. PIMs from *Ma*^{Rg} induces iron accumulation via TLR2-dependent signaling. (A) Wild type and TLR2$^{-/-}$ BMDM cells were treat PIM-F7 (40 ㎍/㎖) directly for 24 h, then cells were stained with FeRhoNox-1 and intracellular iron was quantified under FACS analysis. (B) BMDM cells were treat PIM-F7 (40 ㎍/㎖) directly for 2 h, then infected with *M. abscessus* (MOI=5) for 2 h. Then, cells were washed, and the medium was replaced for 48 h. Cell death was measured by LDH release assay. All data are representative of three independent experiments. In panels A, p-values are indicated (two-way ANOVA). In panel D, p-values are indicated (one-way ANOVA). Error bars represent the mean and standard error of the mean (SEM). n=3.

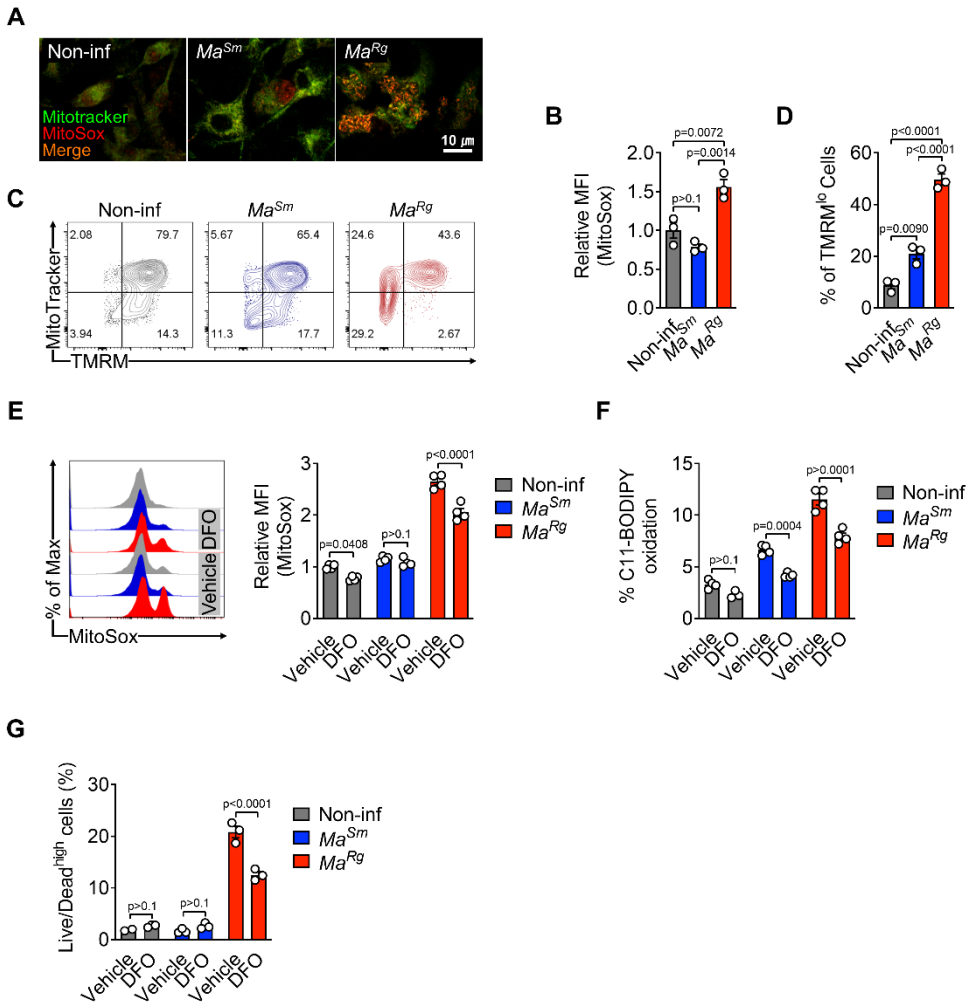

Figure 7. Accumulated iron in *Ma*^{Rg}–infected macrophages drive mitochondrial ROS production. (A) BMDM cells infected with *M. abscessus* (MOI=5) for 2 h, then cells were washed, and the medium was replaced for 12 h. Mitochondrial ROS was stained with MitoSox Red and subjected to fluorescence microscopy. (B) Mitochondrial ROS was quantified under FACS analysis. (C) BMDM cells were infected with *M. abscessus* (MOI=5) for 2 h, then cells were washed, and the medium was replaced for 24 h. Statistics for percentage of

TMRM^{lo}−cells and (D) geometric relative fluorescence intensity was quantified under FACS analysis. BMDM cells infected with *M. abscessus* (MOI=5) after treatment with DFO 1 h. Cells were washed, and the medium was replaced with DFO for 24 h. (E) Mitochondrial ROS production was measured by MitoSox Red staining, (F) Lipid peroxidation was measured by BODIPY C−11 staining, and (G) Cell death was measured by Live/Dead fixable aqua staining using FACS analysis. In panels B and D, p−values are indicated (one−way ANOVA). In panel E−G, p−values are indicated (two−way ANOVA). Error bars represent the mean and standard error of the mean (SEM). n=3−4.

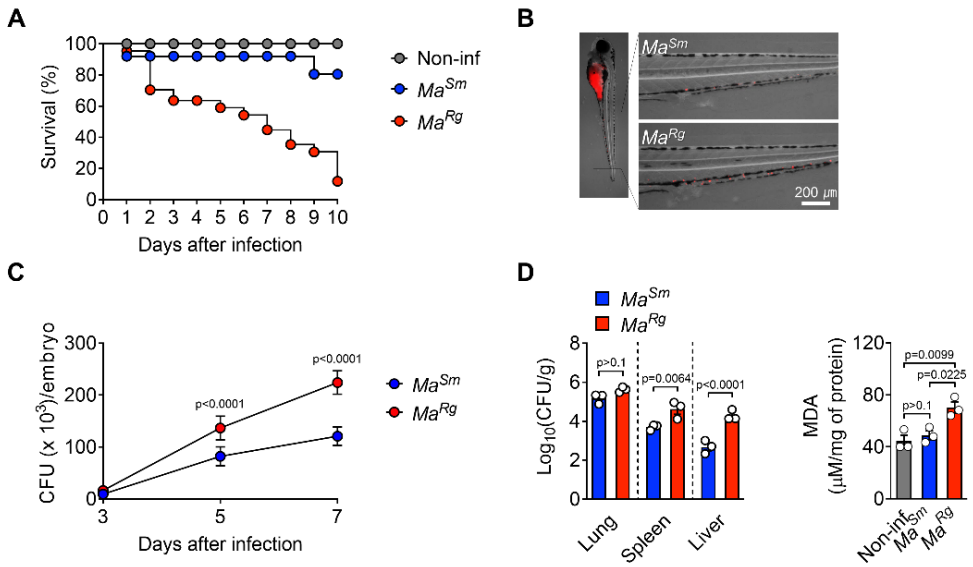

Figure 8. *Ma*^{Rg} induces ferroptosis to promote *Ma*^{Rg} pathogenicity and dissemination *in vivo*. (A) Survival of embryos infected with ~300 colony forming units (CFU) of the *Ma*^{Rg} or *Ma*^{Sm} compared with mock-infected controls (Non-inf) (n=20). Shown are representative results of three independent experiments. Embryos are significantly more susceptible to *Ma*^{Rg} infection than *Ma*^{Sm} infection. (B) Spatiotemporal visualization of the infection by either the DiI-stained *Ma*^{Rg} or the *Ma*^{Sm} (~300 CFU): representative fluorescence and transmission close-up of the tail. (C) Bacterial loads of embryos infected with the *Ma*^{Rg} or the *Ma*^{Sm} (~200 CFU). Embryos infected with *Ma*^{Rg} or *Ma*^{Sm}. Significant expansion of bacterial loads was observed up to 7 dpi within embryos infected with *Ma*^{Rg} or *Ma*^{Sm}. (D) Intranasal inoculation with 1 x 10^6 CFU of *Ma*^{Rg} or *Ma*^{Sm}. CFU were

determined at day 28 after infection by plating serial dilutions of organ homogenates on nutrient 7H11 agar and counting CFU after 3–4 days incubation at 37℃. (n=3 mice in each group). (E) Lipid peroxidation (malondialdehyde) measured in lung homogenates from uninfected and *M. abscessus*–infected mice. All data are representative of three independent experiments. Statistical significance is indicated by p–values (two–way ANOVA), and error bars represent the mean and standard error of the mean (SEM).

Discussion

I previously reported that highly virulent clinical *M. massiliense* strains induce significantly more macrophage extracellular traps than non-virulent strains[40]. Additionally, I observed that the rough morphotype of *M. massiliens* induces necrotic cell death. In the present study, I have discovered that Ma^{Rg} external cell wall lipids promote the dissemination of Ma^{Rg} in the host by inducing ferroptosis through the accumulation of iron. PIM-F7 has shown that iron accumulation interacts with the production of mitochondrial ROS, and that iron chelator inhibits *M. abscessus*-induced ferroptosis. The results demonstrate that the high virulence of Ma^{Rg} is related to the induction of cell death by external cell wall lipids. Various key events of cell death occur in the mitochondria, including the loss of $\Delta\Psi$m and the participation of ROS generation[52-55]. I found that PIM-F7-mediated induction of ferroptosis results in the upregulation of mitochondrial ROS through the accumulation of iron, which leads to the loss of $\Delta\Psi$m.

In addition, I observed increased accumulation of iron in macrophages infected with Ma^{Rg} and treated with PIMs, although the mechanism of PIMs internalization by host cells is remains unknown.

The role of mitochondrial damage in the outcome of macrophage infection by *M. tb* has been suggested in previous studies[56-59]. It has recently been shown that the *M. tb* HBHA protein targets mitochondria and induces mitochondria-dependent cell death in macrophages[60]. My findings indicates that Ma^{Rg} promotes cell death by interacting with accumulated iron to induce mitochondrial ROS. These results suggest that the PIMs of Ma^{Rg} induces ferroptosis by producing mitochondrial ROS through the accumulation of iron, although further study is needed to understand the underlying mechanisms.

Mycobacteria are known to produce a variety of lipids, and in this study, I found that PIM-F7 from the external cell wall lipids is involved in the induction of macrophage ferroptosis. Previous reports have suggested that interaction with PIM2 of *M. abscessus* is required for TLR signaling and activation of the innate immune response[46, 61]. However, my study found that a PIM-F7, rather than PIM2, interacts with TLR2 to induce ferroptosis.

The killing of macrophage is a crucial aspect of host-mycobacterial interactions[62, 63]. The properties of mycobacteria that regulate cell death have been extensively studied, and most reports indicate that the induction of cell death by *M. tb* and *M. avium*

is inversely proportional to bacterial virulence[64]. However, the function of cell death in infection is still a subject of debate. A recently study suggests that *M. tb* induces ferroptosis in macrophages, and that ferroptosis plays an important role in the dissemination of *M. tb*[33]. Although the mechanism by which *M. tb* induces ferroptosis is still unknown, it has been suggested that cell death promote cell-to-cell spread of the bacteria[65-67]. In this study, I found that PIM-F7 induced ferroptosis, which was associated with the spread of bacteria between host cells. Recent research has shown that the proportion of apoptotic macrophages was significantly higher in Ma^{Rg}-infected zebrafish compared to Ma^{Sm}-infected macrophages[47]. My study also found that Ma^{Rg} increased more than Ma^{Sm} in zebrafish infected through the yolk sac, and I observed a similar trend in mice. Consistent with my findings, another study showed that Ma^{Rg} uses ferroptotic macrophages as a vehicle for its spread. However, further studies are needed to investigate whether PIMs can induce ferroptosis in alveolar macrophage in vivo and whether this promotes the spread and growth of Ma^{Rg}.

Chapter 2

Pyruvate dehydrogenase kinase inhibitor Dichloroacetate augments autophagy mediated constraining the replication of *Mycobacteroides massiliense* in macrophages

Introduction

Mycobacteroides abscessus (formerly *Mycobacterium abscessus*) complex is the most common etiological isolate associated with nontuberculous mycobacterial (NTM) pulmonary disease, especially in patients with cystic fibrosis[68]. This species is a rapidly growing mycobacterium with intrinsic and acquired resistance to multidrug-resistant drugs, including macrolides[69]. It shares remarkable similarities in the infection process with slowly growing mycobacteria, such as *Mycobacterium tuberculosis*[4]. The complex consists of three subspecies: *M. abscessus* subsp. *abscessus*, *M. abscessus* subsp. *massiliense*, and *M. abscessus* subsp. *bolletti*[70]. Infections with *M. abscessus* lead to accelerated inflammatory lung damage[71], which are often difficult or impossible to treat despite prolonged courses of combination antibiotics[72-74] and may prevent safe lung transplantation[75, 76]. Therefore, new treatment options are urgently needed to prevent nosocomial transmission and outbreaks[70].

Several host factors affect antimicrobial treatment outcomes and are responsible for disease progression after infection[77]. During the last decade, a renaissance of scientific research strategies

targeting host factors rather than pathogen components has opened up novel treatment approaches, termed host-directed therapy (HDT) [77, 78]. In particular, HDT could be advantageous for treating chronic bacterial infections such as tuberculosis, as it improves host immunity, shortens treatment duration, and reduces antibiotic dose[77-80]. For example, non-steroidal anti-inflammatory drugs are undergoing clinical trials as potential HDTs with actions that improve host bactericidal mechanisms for tuberculosis (NCT02781909, NCT03092817, and NCT02060006). However, the potential effects of HDT have not been reported in treating *M. abscessus*.

Pyruvate dehydrogenase (PDH) is an enzyme complex that plays a central role in aerobic respiration by catalyzing the conversion of pyruvate to acetyl-CoA. This reaction is essential for the citric acid cycle, which generates energy via oxidative phosphorylation (OXPHOS). PDH activity is regulated by pyruvate dehydrogenase kinase (PDK), which phosphorylates and inactivates the enzyme complex[81]. PDKs are a family of mitochondrial enzymes that regulate glucose metabolism and energy production in cells and thus represent a potential target for HDT in several diseases, including cancer, diabetes[82, 83], and infectious diseases[84].

PDK is activated by high levels of ATP, NADH, and acetyl-CoA; however, when energy demands increase, PDK activity is inhibited by small-molecule compounds known as PDK inhibitors. According to a previous study, PDK is upregulated in macrophages infected with *Salmonella enterica s*erovar *typhimurium*, and inhibition of PDK using dichloroacetate (DCA) increases the production of reactive oxygen species and decreases the production of pro-inflammatory cytokines, but not in *M. tuberculosis*[85].

This study found that *M. massiliense* infection-induced metabolic rewiring in macrophages could be reversed by inhibiting PDK with DCA. Autophagy and phagolysosomal fusion were induced by DCA treatment, thus leading to constraining intracellular replication of *M. massiliense* in macrophages. Our findings suggest that DCA is a potential HDT candidate for controlling *M. massiliense* infection.

Materials and methods

Reagents and antibodies

Dimethyl sulfoxide, 2-deoxy-D-glucose, D-(+)-glucose, D-(+)-galactose, sodium DCA, wortmannin, and phorbol 12-myristate 13-acetate (PMA) were obtained from Sigma-Aldrich (St. Louis, MO, USA). Carbonyl cyanide, 4-(trifluoromethoxy) phenylhydrazone, was obtained from Seahorse Bioscience (Billerica, MA, USA). Anti-phospho-AMPKα (THR172; cat. no. 2535) and anti-AMPKα (cat. no. 2532) were purchased from Cell Signaling Technology (Danvers, MA, USA), and anti-mTOR (phospho S2448; cat. no. ab109268) antibodies were purchased from Abcam (Cambridge, UK). Anti-mTOR (cat. no. sc-517464), anti-β-actin (cat. no. sc-47778), and control siRNA A A (cat. no. sc-37007), and human AMPKα1/2 siRNA (cat. no. sc-453120) were purchased from Santa Cruz Biotechnology (Dallas, TX, USA). Anti-LC3II was purchased from Sigma-Aldrich. Secondary stabilized peroxidase-conjugated goat anti-rabbit IgG (H+L) and goat anti-mouse IgG (H+L) were purchased from Thermo Fisher Scientific (Waltham, MA, USA).

Bacterial culture

A clinically isolated rough strain of the *M. massiliense* rough variant belonging to *M. massiliense* Asan 50594 of the type II genotype was used in this study. *M. massiliense* was cultured in Middlebrook 7H9 medium (BD Biosciences, Franklin Lakes, NJ, USA) supplemented with 10% ADC, 0.2% glycerol, and 0.05% Tween 80 (Sigma-Aldrich). The cultured bacteria were collected via centrifugation. The collected mycobacteria were stored at –80℃ until use. To prepare single cells of *M. massiliense*, cultured bacteria were homogenized with a 23-gauge syringe needle for 10 min after soft-spin centrifugation to exclude bacterial clumping. The number of viable bacteria in the stored bacterial vials was counted on Luria-Bertani (LB) agar (BD Biosciences).

Cell culture

The human acute monocytic leukemia THP-1 (ATCC TIB-202) cell line was obtained from the ATCC and maintained in RPMI medium (Welgene, Gyeongsangbuk-do, South Korea) containing 10% fetal bovine serum (FBS; Gibco, Billings, MT, USA) and 1% penicillin-streptomycin (PS; Gibco). THP-1 cells were differentiated into macrophages by incubation with 50 ng/ml PMA for 2 days. The medium was then replaced with a medium without 1% PS for 1 day.

PMA-differentiated THP-1 cells were infected with *M. massiliense* at a multiplicity of infection (MOI) of 1 for 1 hour, and the medium was replaced to establish *M. massiliense* infection. To quantify the colony-forming units (CFUs), infected cells were lysed in PBS containing 0.1% Triton X-100 and plated on LB agar.

Bone marrow-derived macrophages (BMDMs) were obtained from C57BL/6J male mice at 7-12 weeks of age and were differentiated by bone marrow cell culture for 5 days in complete RPMI containing 10% FBS, 20% L929 cell-conditioned medium, 1% PS, and 2 mM L-glutamine. Mature BMDMs were scraped from dishes, reseeded at a density of 2×10^5 cells per well in 24-well plates in antibiotic-free complete medium, and allowed to rest for 2 days. All cells were cultured at 37℃ in a humidified incubator containing 5% CO_2. AMPK $\alpha^{-/-}$ mice were provided by Dr. B. Viollet (INSERM U1016, Institut Cochin, Paris, France) and used as a source of bone marrow cells.

CFU assays

For in vitro CFU assays, BMDMs were infected for 1 h with *M. massiliense*, washed with PBS, and harvested in fresh medium. At 1 dpi, the cells were lysed with 500 ml of 1% Triton X-100 for 10 min

to release intracellular bacteria and then serially diluted with PBST. The lysed cells were plated on LB agar Petri dishes. Bacterial colonies were counted after 3-4 days of incubation at 37℃.

Measuring cellular metabolic flux

An XFe24 Extracellular Flux Analyzer (Seahorse Bioscience) was used to determine the bioenergetic profile of intact cells. Briefly, PMA-differentiated THP-1 cells and BMDMs were differentiated in XFe24 analyzing plates. Before data acquisition, the medium was replaced with high-glucose Dulbecco's modified Eagle medium (Sigma-Aldrich) supplemented with 1 mM sodium pyruvate (Sigma-Aldrich) and 10% FBS. The extracellular acidification rate (ECAR) and oxygen consumption rate (OCR) were analyzed after 3 h.

RNA extraction and quantitative real-time PCR analysis

Total RNA was extracted using the TRIzol reagent (Invitrogen, Waltham, MA, USA) according to the manufacturer's instructions.

Complementary DNA was synthesized from total RNA by reverse transcription, and the amount of mRNA was determined by real-time PCR analysis using SYBR Green qPCR PreMix (Enzynomics, Daejeon, South Korea) on an ABI real-time PCR 7500 machine (Applied

Biosystems, Waltham, MA, USA). Samples were normalized to the β-actin levels. PCRs were performed using primers for *TFEB* (forward, 5′-CCA GAA GCG AGA GCT CAC AGA T-3′; reverse, 5′-TGT GAT TGT CTT TCT TCT GCC G-3′), *SQSTM1* (forward, 5′-GCA CCC CAA TGT GAT CTG C-3′; reverse, 5′- CGC TAC ACA AGT CGT AGT CTG G-3′), *BECN 1* (forward, 5′- ACC GTG TCA CCA TCC AGG AA-3′; reverse, 5′- GAA GCT GTT GGC ACT TTC TGT-3′), *CTSD* (forward. 5′-AAC TGC TGG ACA TCG CTT GCT-3′; reverse, 5′-CAT TCT TCA CGT AGG TGC TGG A-3′), *MAP1LC3A* (forward, 5′- GAG AAG CAG CTT CCT GTT CTG G-3′; reverse, 5′- GTG TCC GTT CAC CAA CAG GAA G-3′), *LAMP1* (forward, 5′- ACG TTA CAG CGT CCA GCT CAT-3′; reverse, 5′-TCT TTG GAG CTC GCA TTG G-3′), and *LAMP2* (forward, 5′-TGC TGG CTA CCA TGG GGC TG-3′; reverse, 5′-GCA GCT GCC TGT GGA GTG AGT-3′).

Western blot analysis

Total cell lysates were prepared by harvesting the cells in sample buffer (Biosesang, Gyeonggi-do, Korea) with protease and phosphatase inhibitors (GenDEPOT, Katy, TX, USA), sonicated for 40 s, and heated to 99℃ for 5 min. Proteins were resolved on 12%

polyacrylamide gels and transferred to polyvinylidene difluoride membranes (Merck Millipore, Burlington, MA, USA).

AMP/ATP measurement

Total cell lysates were prepared by harvesting the cells in ultrapure water (Invitrogen) and quickly homogenizing them by sonication. After centrifugation for 5 min at 4℃ at 13,000×g, the supernatant was deproteinized using 4 M perchloric acid and neutralized using 2 M KCl. The AMP-Glo™ Assay and ENLITEN® ATP Assay System (both from Promega, Madison, WI, USA) were used to measure the amount of ATP and AMP in the cell lysates.

Transfection and siRNA-mediated knockdown

PMA-differentiated THP-1 macrophages and BMDMs were transfected with the purified EGFP-LC3 expression plasmid using the Lipofectamine® 3000 transfection reagent (Invitrogen). PMA-differentiated THP-1 macrophages with siRNA knockdown were treated with Lifofectamine® RNAiMAX. Transfection was performed using Opti-MEM (Thermo Fisher Scientific) according to the manufacturer's protocol. After transfection, the cells were treated with DCA and challenged with *M. massiliense* to assess intracellular

bacterial killing and autophagy-related protein expression. Fluorescence was observed using a fluorescence microscope CTR6000 (Leica, Wetzlar, Germany). For the quantification of LC3 puncta per cell, three individual images per sample were counted.

LysoTracker staining

PMA-differentiated THP-1 macrophages were cultured on 12-mm glass cover slides in 24-well plates (2×10^5 cells per well) and infected with *M. massiliense* (MOI=1) with or without 40 mM DCA for 24 hours. Cells were incubated with 5 μM LysoTracker red (Invitrogen) for 30 min at 37℃. Fluorescence was observed using a Leica TCS SP8 confocal microscope (Leica Microsystems). The LysoTracker-*M. massiliense* colocalization ratio was calculated from three individual images per sample.

Statistical analysis

All statistical analyses were performed using GraphPad Prism version 8.0 (GraphPad, San Diego, CA, USA) and are shown as mean ± standard error of the mean (SEM).

Results

Blocking PDK activity by DCA treatment rewires the metabolic state of *M. massiliense*–infected macrophages and restricts bacterial growth

I have previously reported the role of PDK in increasing glycolysis in lipopolysaccharide–stimulated macrophages[86]. Similarly, intracellular growth of *S. enterica s*erovar *typhimurium* induces glycolysis in human macrophages, and inhibition of PDK activity by DCA treatment restricts bacterial replication[85]. To investigate whether DCA can control intracellular *M. massiliense*, I first determined the metabolic changes in *M. massiliense*–infected macrophages with or without DCA treatment. The ECAR and OCR were measured as indicators of the glycolytic and OXPHOS energy phenotypes, respectively. As expected, *M. massiliense* infection induced a metabolic shift toward a more glycolytic phenotype, accompanied by increased glycolysis, glycolytic capacity, and glycolytic reserve in PMA–differentiated THP–1 macrophages (Fig. 1A and B). Pretreatment with 40 mM DCA significantly reduced ECAR (Fig. 1A and B), indicating the involvement of PDK in the glycolytic changes in *M. massiliense*–infected macrophages. OCR

was not affected by *M. massiliense* infection. However, DCA treatment further increased the basal and maximal respiration in *M. massiliense*-infected macrophages (Fig. 1C and D). Consequently, the OCR/ECAR ratio was significantly increased in DCA-treated *M. massiliense*-infected macrophages (Fig. 1E). DCA also affected intracellular *M. massiliense* survival, showing dose-dependent restriction of bacterial growth in both THP-1 (Fig. 1F) and mouse BMDMs (Fig. 1G). Blocking glycolysis by 2-deoxyglucose (2-DG) treatment restricted *M. massiliense* replication (Fig. 1H), further supporting the idea that *M. massiliense* requires host glycolysis for proliferation. In addition, as glycolysis was reported to be related to pro-inflammatory cytokine synthesis in macrophages[87], *M. massiliense* infection increased tumor necrosis factor α production, whereas blocking glycolysis by DCA treatment significantly reversed this increase (Fig. 1I). DCA alone did not alter the viability of macrophages or bacterial growth (Fig. 2), nor did it induce cytokine responses (data not shown). Collectively, these results suggest that DCA exerts its antimicrobial activity against *M. massiliense* by inducing host metabolic shifts.

DCA reduced intracellular *M. massiliense* replication via AMPKα1

phosphorylation in macrophages

As shown in our previous study, blocking PDK activity in stimulated macrophages could lead to the phosphorylation of AMPKα1 due to an increased AMP/ATP ratio[86]. To determine whether AMPK is required for the DCA-driven metabolic switch, I first measured the ECAR and OCR of *M. massiliense*-infected macrophages with and without DCA treatment as indicators of the glycolytic and OXPHOS energetic phenotypes, respectively, in cells from BMDMs isolated from wild-type and AMPKα1-deficient mice. Interestingly, both glycolysis and OXPHOS were reduced in BMDMs isolated from AMPKα1-deficient mice (Fig. 3). AMPKα1 deficiency significantly abrogated infection-mediated increase of glycolysis (Fig. 3A and B), whereas DCA further reduces the ECAR of *M. massiliense*-infected AMPKα1-deficient macrophages. This result demonstrated the strong involvement of AMPKα1 in glycolytic changes by *M. massiliense* infection, with partial AMPKα1-independent action of PDK. In case of OCR, decrease by infection and recovery by DCA treatment were completely abolished in AMPKα1-deficient BMDMs, indicating the essential role of AMPK in the metabolic changes of DCA-treated *M. massiliense*-infected macrophages.

To investigate whether the DCA treatment's restriction of

bacterial growth is also involved with the AMPK α1, I first measured the AMP/ATP ratio (Fig. 4A). Similar to the lipopolysaccharide-stimulated macrophages, DCA treatment increased the AMP/ATP ratio in *M. massiliense*-infected macrophages. I also found that DCA treatment increased AMPK α1 phosphorylation at Thr172 in THP-1 cells (Fig. 4B), which was repeated in BMDMs obtained from WT mice but completely abrogated in BMDMs obtained from AMPK α1-deficient mice (Fig. 4C). To determine whether AMPK α1 has a role in the effect of DCA on *M. massiliense* growth, I compared intracellular bacterial replication in BMDMs isolated from wild-type and AMPK α1-deficient mice (Fig. 4C). As a result, restriction of bacterial growth was only observed in BMDMs from WT mice, not from KO mice (Fig. 4D), indicating that AMPK α1 is involved in its mode of action. These results were recapitulated in the human macrophages in that AMPK α1 knockdown using siRNA-abrogated DCA-mediated AMPK α1 phosphorylation (Fig. 4E) and killing of *M. massiliense* in macrophages (Fig. 4F).

DCA-induced autophagy and lysosomal gene expression

Several studies have reported the involvement of AMPK α1 in autophagy[88, 89] and autophagy-induced antimicrobial effect in

macrophages[90-92]. In *M. massiliense*-infected macrophages, LC3II expression (Fig. 5A) and punctate structures (Fig. 5B) were significantly increased only in DCA-pretreated cells. To further confirm the role of AMPKα1 in autophagosome formation, I compared the LC3II expression and numbers of LC3 puncta in wild-type and AMPKα1$^{-/-}$ BMDMs. DCA treatment did not significantly increase LC3II expression in AMPKα1-deficient BMDMs (Fig. 5C and D), indicating that AMPKα1 significantly contributes to autophagosome formation. Moreover, DCA increased mRNA levels of the transcription factor EB (TFEB), which is critical for innate host defense against *M. massiliense* infection (Fig. 6A)[93]. Consistent with these data, genes downstream of TFEB, including *SQSTM1*, *BECN1*, and *CTSD*, were markedly upregulated by DCA in infected macrophages (Fig. 5A). I also found that DCA significantly increased the mRNA expression of autophagy and lysosomal genes such as *MAP1LC3A*, *LAMP1*, and *LAMP2* (Fig. 6A). These data suggested that DCA promotes lysosomal gene expression by inducing TFEB activation in macrophages during *M. massiliense* infection.

It has been well described that the induction of acidification within phagocytic cells, i.e., phagosomal colocalization with the lysosomal marker LAMP1, is essential for host defense against

M. abscessus infection in BMDMs[94]. Therefore, I investigated whether DCA could upregulate the co-localization of phagosomes and lysosomes. To this end, I analyzed the colonization of lysosome-bearing bacterial phagocytic cells using confocal imaging (Fig. 6B). Interestingly, DCA significantly increased the co-localization of *M. massiliense* and lysosomes in macrophages at 24 hpi (Fig. 6B). The inhibition of autophagy with wortmannin restored intracellular bacterial growth to a level comparable to that of DCA-untreated macrophages (Fig. 6C). These results strongly suggest that DCA significantly induces self-trapping or lysosomal gene expression and activity during *M. massiliense* infection.

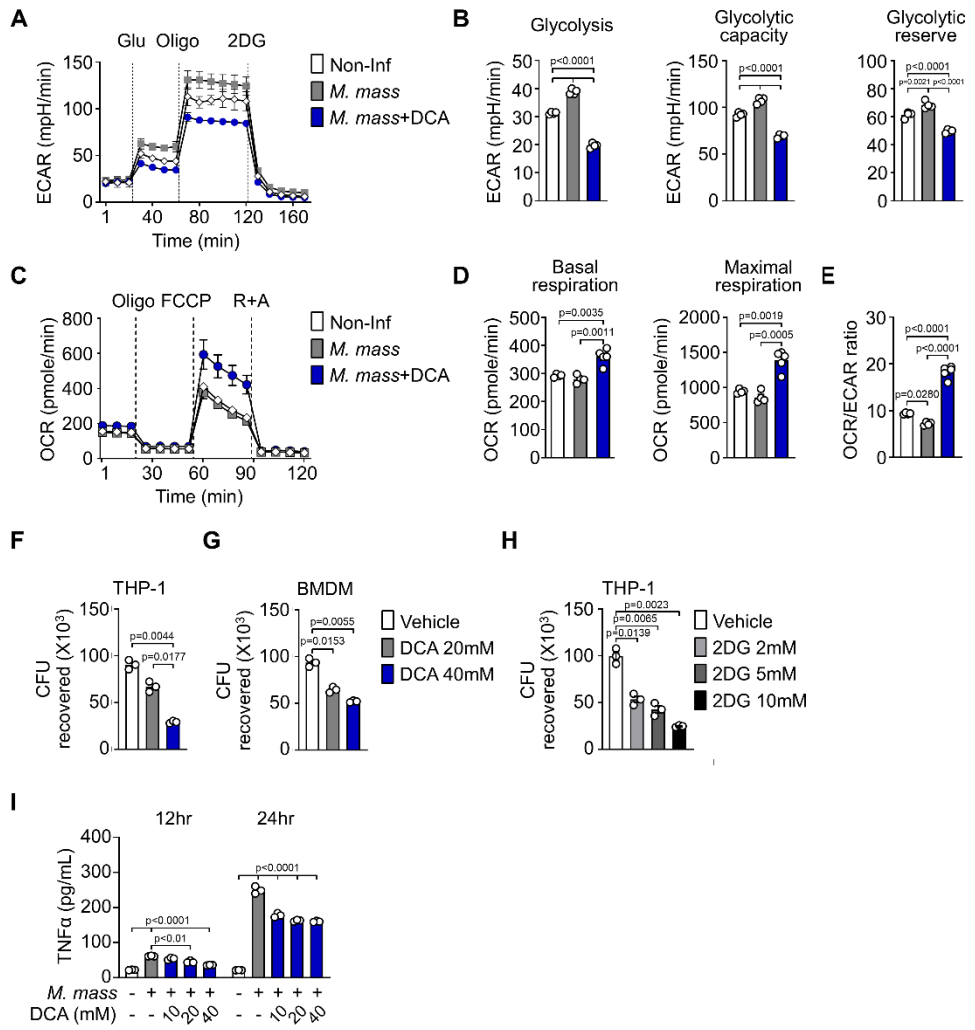

Figure 1. DCA decreased glycolysis and intracellular *M. massiliense* in macrophages. (A–D) Differentiated THP-1 macrophages treated with DCA (40 mM) for 1 h followed by infection with *M. massiliense* (MOI=1). ECAR and OCR were measured 2 h post-infection. (A) ECAR recorded with sequential treatments of glucose (10 mM), oligomycin (10 μM), and 2-DG (100 mM). (B) Glycolysis, glycolytic capacity, and glycolytic reserve obtained from (A). (C) The OCR was

recorded with sequential treatments of oligomycin (2.5 μM), FCCP (2 μM), and rotenone with ATP (0.5 μM). (D) Basal and maximal respiration calculated from (C). (E) OCR/ECAR ratio. CFUs recovered at 24 h post-infection in differentiated THP-1 macrophages (F) and BMDMs (G). (H) CFUs in differentiated THP-1 macrophages at 24 h post-infection with or without 2-DG. (I) Tumor necrosis factor α production measured by enzyme-linked immunoassay in the culture supernatant. Cells were infected with *M. massiliense* (MOI=1) for the indicated time points. DCA was pretreated 1 h before *M. massiliense* infection with the indicated concentrations. All data are representative of three independent experiments. In panels B and D-H, p-values are indicated (one-way ANOVA). In panel I, p-values are indicated (two-way ANOVA). Error bars represent the mean and standard error of the mean (SEM). n=3-5.

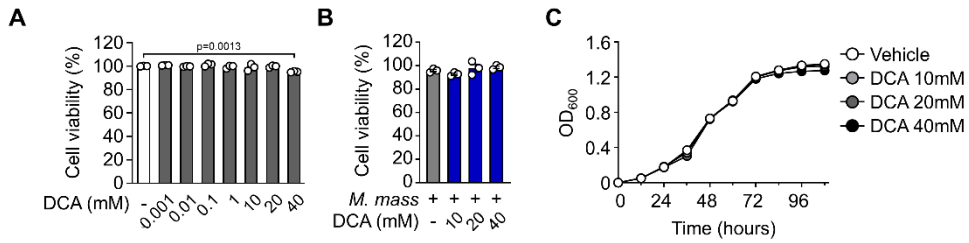

Figure 2. DCA alone had no effect on macrophage viability, bacterial growth. (A) Differentiated THP-1 macrophages were treated with DCA in dose-dependent manner, ranging from 0.01 to 40 mM, for 24 h. (B) After pre-treated with DCA (10, 20, and 40 mM) for 1 h, macrophages were infected with *M. massiliense* (MOI=1) for 2 h. Following this, the cells were washed, and the medium was replaced with fresh DCA-containing medium for 24 h. Cell viability was assessed using a CCK-8 assay kit. (C) *M. massiliense* in 7H9 Broth (with 10% ADC) was incubated at 37℃ with various concentrations of DCA (0, 10, 20, and 40 mM). Growth curve analysis was performed by measuring the OD600 at regular intervals over a period of 108 h. Statistical significance is indicated by p-values (one-way ANOVA), and error bars represent the mean and standard error of the mean (SEM). n=3.

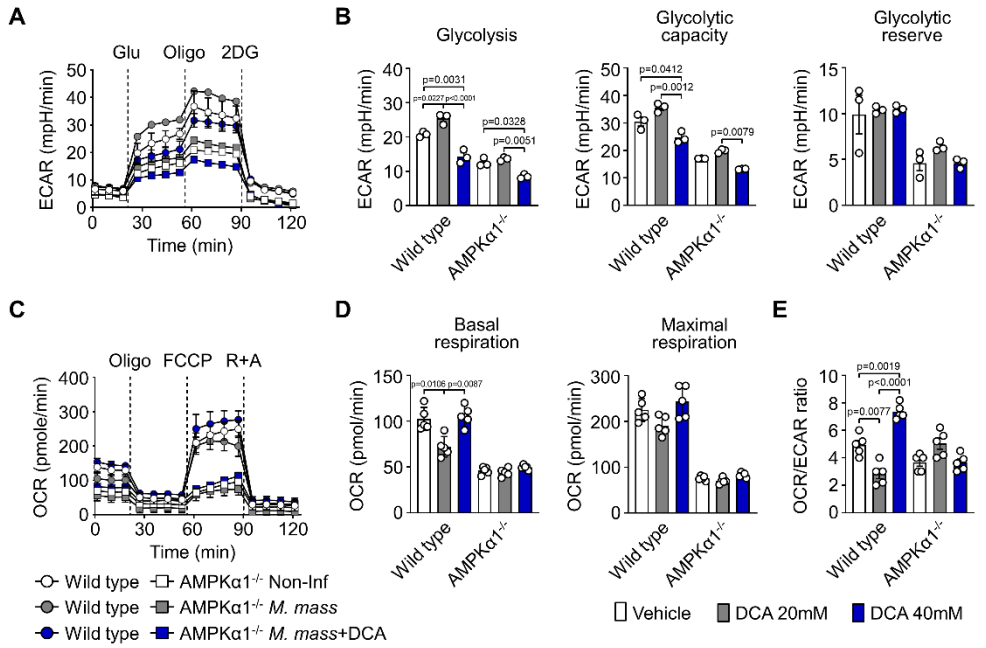

Figure 3. AMPKa1 deficiency impairs glycolytic and OXPHOS activity in macrophages. Wild-type and AMPK$\alpha 1^{-/-}$ BMDMs were treated with DCA (40 mM) for 1 h followed by infection with *M. massiliense* (MOI=1). ECAR and OCR were measured 2 h post-infection. (A) ECAR recorded with sequential treatments of glucose (10 mM), oligomycin (10 μM), and 2-DG (100 mM). (B) Glycolysis, glycolytic capacity, and glycolytic reserve obtained from (A). (C) OCR recorded with sequential treatments of oligomycin (2.5 μM), FCCP (2 μM), and rotenone with ATP (0.5 μM). (D) Basal respiration and maximal respiration calculated from (C). (E) OCR/ECAR ratio. All data are representative of three independent experiments. Statistical significance is indicated by p-values (two-way ANOVA), and error

bars represent the mean and standard error of the mean (SEM). n=3-5.

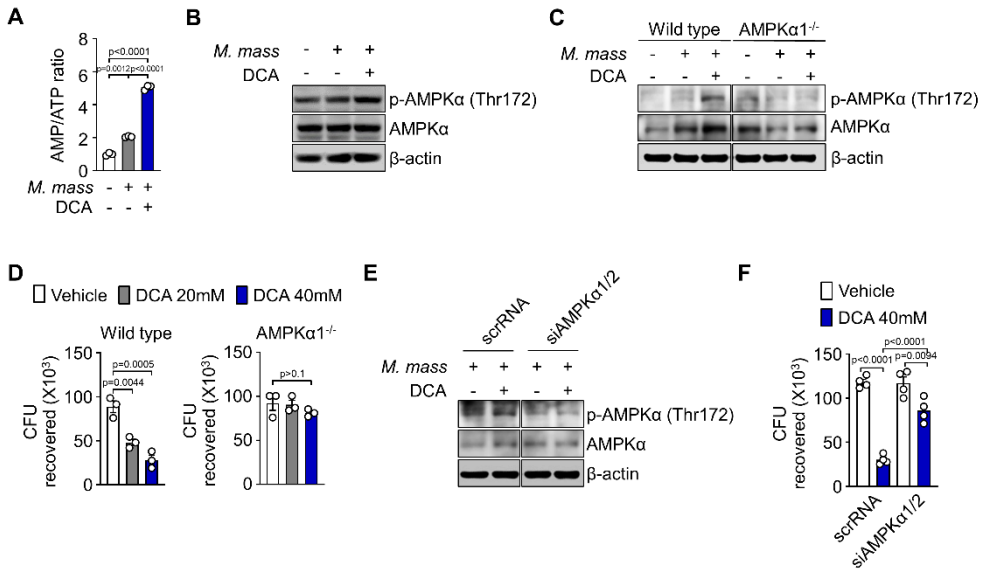

Figure 4. DCA increased phosphorylated AMPKα1 in *M. massiliense*-infected macrophages. (A) Differentiated THP-1 macrophages infected with *M. massiliense* (MOI=1) after DCA (40 mM) treatment. Cells were washed, and the medium was replaced with DCA (40 mM) for 4 h. AMP/ATP ratio changed in differentiated THP-1 macrophages by DCA treatment determined using a luminescence-based detection kit. (B) Immunoblot analysis of phosphorylated AMPKα1 and total AMPKα in differentiated THP-1 macrophages. (C) AMPKα1 protein level determined by immunoblot analysis from BMDMs of wild-type or AMPK$\alpha 1^{-/-}$ mice, which were treated with DCA (40 mM) 1 h, followed by infection with *M. massiliense* (MOI=1) for 1 h and then washed; the medium was replaced with DCA for 24 h. (D) CFUs recovered from BMDMs. (E)

AMPKα protein level determined by immunoblot analysis from differentiated THP−1 macrophages, transfected with scramble RNA and siRNA AMPKα1/2, and treated with DCA (40 mM) 1 h followed by infection with *M. massiliense* (MOI=1) for 24 h. (F) CFUs recovered from differentiated THP−1 macrophages. All data are representative of three independent experiments. In panels A and D, p−values are indicated (one−way ANOVA). In panel F, p−values are indicated (two−way ANOVA). Error bars represent the mean and standard error of the mean (SEM). n=3−4.

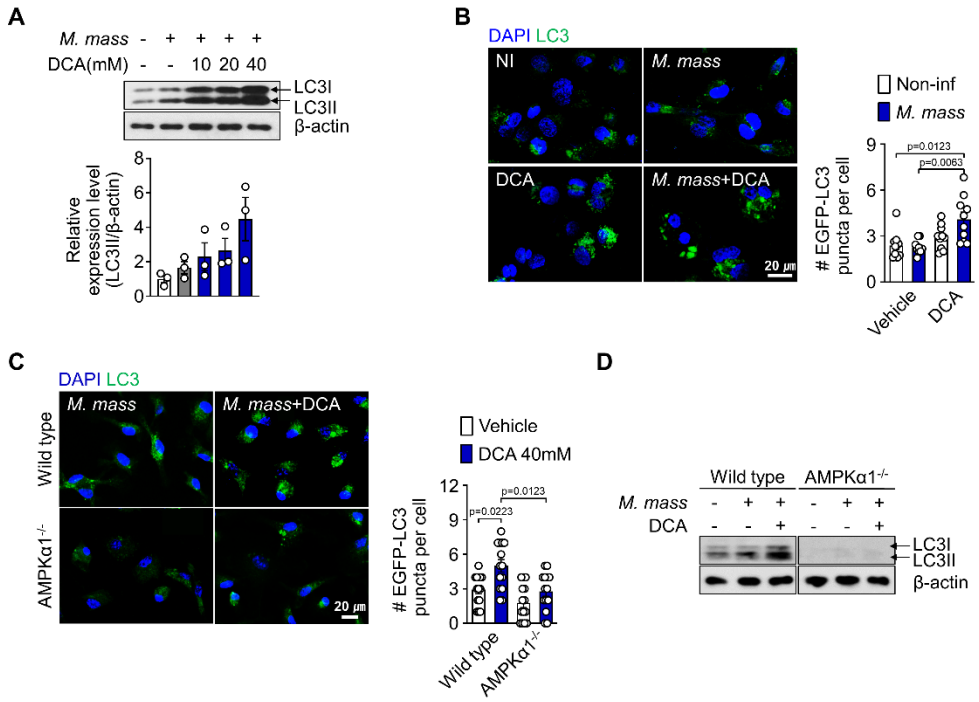

Figure 5. DCA-induced autophagy enhances clearance of intracellular *M. massiliense* in macrophages. (A) Protein expression of LC3 in differentiated THP-1 macrophages was determined using Western blot analysis. (Top) Representative blot from one out of three independent experiments; (bottom) band intensities quantified using Fiji/ImageJ. Cells were treated with DCA (10, 20, or 40 mM) for 1 h, followed by infection with *M. massiliense* (MOI=1) for 1 h and then washed; the medium was replaced with DCA for 24 h. (B) Differentiated THP-1 macrophages transfected with EGFP-LC3 expression plasmid were treated with DCA (40 mM) for 1 h followed by infection with *M. massiliense* (MOI=1) for 24 h, and the EGFP-LC3 puncta per cell were counted under fluorescence microscopy.

Scale bars, 20 μm. (C) BMDMs of wild-type or AMPK$\alpha 1^{-/-}$ mice transfected with EGFP-LC3 expression plasmid were treated with DCA (40 mM) for 1 h followed by infection with *M. massiliense* (MOI=1) for 24 h, and the EGFP-LC3 puncta per cell were counted using fluorescence microscopy. Quantification was performed from three experiments, with 10 images quantified for each condition. Scale bars, 20 μm. (D) Protein expression of LC3 in BMDMs determined using Western blot analysis. Cells were treated with DCA (40 mM) for 1 h, followed by infection with *M. massiliense* (MOI=1) for 1 h and then washed; the medium was replaced with DCA for 24 h. All data are representative of three independent experiments. In panels B and D-H, p-values are indicated (two-way ANOVA). In panel A, p-values are indicated (one-way ANOVA). Error bars represent the mean and standard error of the mean (SEM). n=3.

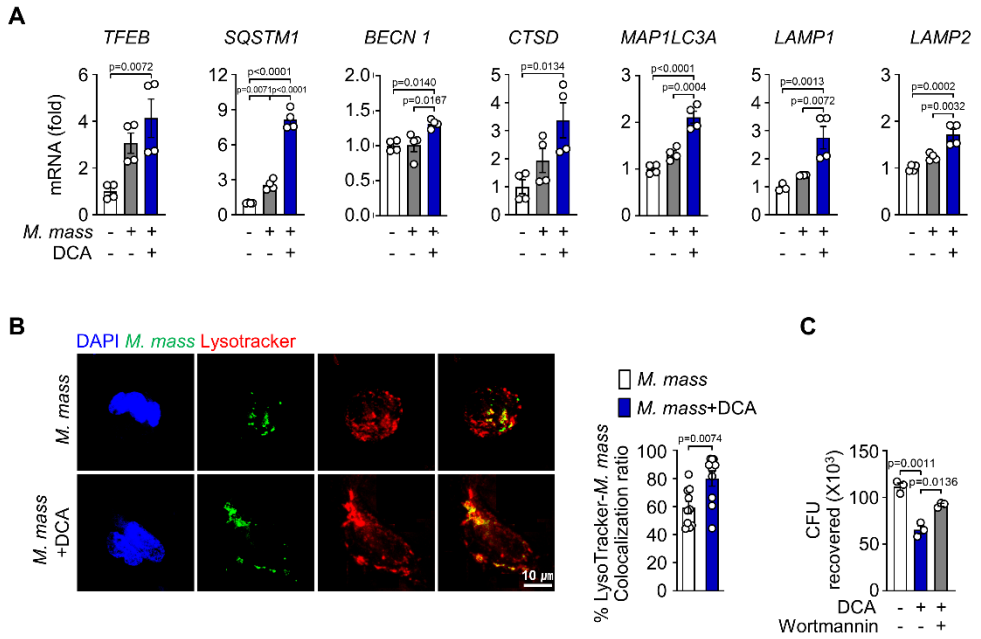

Figure 6. DCA increased the colocalization of phagosomes and lysosomes against *M. massiliense* infection. (A) Cells were lysed, total RNAs were extracted, and the expression of *TFEB*, *SQSTM1*, *BECN 1*, *CTSD*, *MAP1LC3A*, *LAMP1*, and *LAMP2* at mRNA level was determined by qRT-PCR. Cells were pretreated with DCA 40 mM for 1 h, infected with *M. massiliense* (MOI=1) for 1 h, and then washed; the medium was replaced with DCA for 24 h. (B) Differentiated THP-1 macrophages were treated with DCA (40 mM) for 1 h followed by infected with CFSE-stained *M. massiliense* (green) (MOI=1) for 1 h. Then, the cells were washed, and the medium was replaced with DCA for 24 h. Then, cells were stained with LysoTracker (red) and subjected to fluorescence microscopy. Scale

bars, 10 μm. The quantitative data of colocalization of LysoTracker and *M. massiliense* are presented (n=10 for each group). (C) CFUs recovered from differentiated THP-1 macrophages were treated with DCA (40 mM) alone or DCA+wortmannin (20 μM) followed by infection with *M. massiliense* (MOI=1) for 24 h. All data are representative of three independent experiments. In panels A and C, p-values are indicated (one-way ANOVA). In panel B, p-values are indicated (unpaired t-test). Error bars represent the mean and standard error of the mean (SEM). n=3.

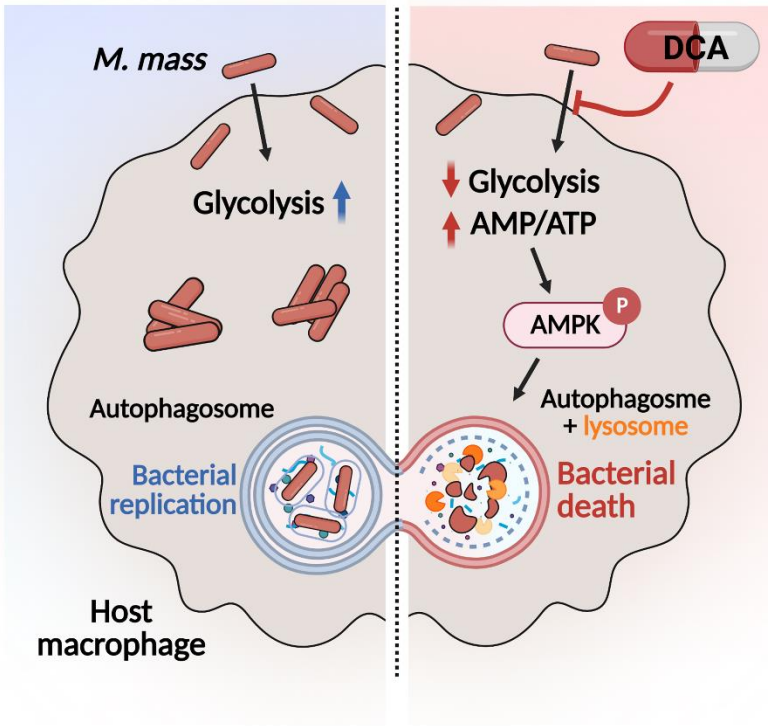

Figure 7. Schematic depiction of DCA-induced autophagy on *M. massiliense* infection. DCA converts increased glycolysis and promotes AMPK α1 phosphorylation, thereby inducing autolysosome maturation in macrophages.

Discussion

Understanding pathogen-specific immune responses is essential for developing appropriate HDT. Here, I show that *M. massiliense*, one of the second-most common pathogenic pulmonary diseases caused by NTM, increases the glycolysis of host macrophages in a PDK-dependent manner. The PDK inhibitor DCA, a novel candidate for HDT against *M. massiliense*, effectively constrained intracellular bacterial replication by potentiating host autophagy and phagolysosomal fusion (Fig. 7).

M. massiliense and *M. tuberculosis* share standard features but interact differently with host cell metabolism. Although *M. tuberculosis* induces a shift from OXPHOS to aerobic glycolysis in human alveolar macrophages, this metabolic change is required to restrict bacillary survival by producing interleukin 1β [95]. *M. tuberculosis*-induced miR-21 expression has been suggested to inhibit host glycolysis and lead to bacterial replication [96]. In contrast, our results showed a completely different behavior of *M. massiliense* from *M. tuberculosis* in response to the host immunometabolic states. Complex factors, including pathogen-intrinsic virulence genes and immune evasion mechanisms, may determine the outcomes in a specific manner.

I found that *M. massiliense* induces rapid upregulation of glycolysis in macrophages providing energy rapidly to sustain the biosynthesis of inflammatory molecules during the early stages of infection[95, 97-101]. Our findings suggest that DCA effectively decreases the ECAR and increases the OCR in *M. massiliense*-infected macrophages. *M. massiliense* infection markedly increases the AMP/ATP ratio, activates AMPK phosphorylation, and induces autophagy. AMPK acts as a metabolic checkpoint that inhibits cell growth under nutrient-deprived conditions. The most specific mechanism by which AMPK regulates cell growth is the suppression of the mTORC1 pathway[102]. AMPK downregulates mTOR activity, and the dephosphorylation of mTORC1 targets FOXK1, FOXK2, and TFEB. As a result, it allows for increased transcription of autophagy genes downstream of FOXO3 binding[89]. AMPK inhibition by mTOR allows sufficient levels of *Tfeb* to enter the nucleus and transcriptionally upregulate the endolysosomes[103]. Our data partly agree with recent data showing that DCA upregulates lysosome-related gene expression and induces autophagy[104, 105]. Together with the current findings, a shift in metabolic changes during antibiotic treatment may also contribute to integrated host responses during chemotherapy against chronic infections. Previous

studies have suggested that antibiotics such as azithromycin aggravate the impairment of autophagy during *M. abscessus* infection, predisposing patients with cystic fibrosis to NTM infections. Mechanistically, the long-term use of the macrolide drug azithromycin inhibits the intracellular clearance of *M. abscessus* in human macrophages, at least because of defective autophagy and the prevention of lysosomal acidification of NTM bacteria[106]. However, a recent report has shown that treatment with autophagy inhibitors and activators (chloroquine and rapamycin, respectively) does not promote antimycobacterial effects against *M. abscessus* rough- and smooth-variant infections in neutrophils[107]. Therefore, further studies are required to determine the exact roles and mechanisms by which autophagy activation regulates the virulence or protective responses during *M. abscessus* infection.

Treating NTM infections is challenging because it requires multidrug regimens for at least 18 months and is often associated with severe side effects and drug resistance[108, 109]. This explains the need to develop new drugs to promote host immune responses and enhance antimicrobial activity against *M. massiliense* infection. Thus, the present findings strongly support the potential of DCA as a drug candidate for the enhanced killing of *M. massiliense*

by macrophages.

Reference

1. Tortoli, E., *Microbiological features and clinical relevance of new species of the genus Mycobacterium.* Clinical microbiology reviews, 2014. **27**(4): p. 727-752.
2. Tortoli, E., et al., *The new phylogeny of the genus Mycobacterium: the old and the news.* Infection, Genetics and Evolution, 2017. **56**: p. 19-25.
3. Turenne, C.Y., *Nontuberculous mycobacteria: Insights on taxonomy and evolution.* Infection, Genetics and Evolution, 2019. **72**: p. 159-168.
4. Johansen, M.D., J.-L. Herrmann, and L. Kremer, *Non-tuberculous mycobacteria and the rise of Mycobacterium abscessus.* Nature Reviews Microbiology, 2020. **18**(7): p. 392-407.
5. Angenent, L.T., et al., *Molecular identification of potential pathogens in water and air of a hospital therapy pool.* Proceedings of the National Academy of Sciences, 2005. **102**(13): p. 4860-4865.
6. Falkinham III, J.O., et al., *Mycobacterium avium in a shower linked to pulmonary disease.* Journal of water and health, 2008. **6**(2): p. 209-213.
7. Falkinham, J.O., *Environmental sources of nontuberculous mycobacteria.* Clinics in chest medicine, 2015. **36**(1): p. 35-41.
8. Runyon, E.H., *Anonymous mycobacteria in pulmonary disease.* 1959.
9. Wolinsky, E., *Mycobacterial diseases other than tuberculosis.* Clinical Infectious Diseases, 1992. **15**(1): p. 1-12.
10. Swenson, C., C.S. Zerbe, and K. Fennelly, *Host variability in NTM disease: implications for research needs.* Frontiers in microbiology, 2018. **9**: p. 2901.
11. Simons, S., et al., *Nontuberculous mycobacteria in respiratory tract infections, eastern Asia.* Emerging infectious diseases, 2011. **17**(3): p. 343.
12. Medjahed, H., J.-L. Gaillard, and J.-M. Reyrat, *Mycobacterium abscessus: a new player in the mycobacterial field.* Trends in microbiology, 2010. **18**(3): p. 117-123.
13. Nessar, R., et al., *Mycobacterium abscessus: a new antibiotic nightmare.* Journal of antimicrobial chemotherapy, 2012. **67**(4): p. 810-818.
14. Leung, J.M. and K.N. Olivier. *Nontuberculous mycobacteria in patients with cystic fibrosis*. in *Seminars in respiratory and critical care medicine*. 2013. Thieme Medical Publishers.
15. Park, I.K. and K.N. Olivier. *Nontuberculous mycobacteria in cystic fibrosis and non-cystic fibrosis bronchiectasis*. in *Seminars in respiratory and critical care medicine*. 2015. Thieme Medical Publishers.
16. Chan, E.D., et al., *Host immune response to rapidly growing*

mycobacteria, an emerging cause of chronic lung disease. American journal of respiratory cell and molecular biology, 2010. **43**(4): p. 387-393.
17. Moore, M. and J.B. Frerichs, *An Unusual Acid-Fast Infection of the Knee with Subcutaneous, Abscess-Like Lesions of the Gluteal Region: Report of a Case with a Study of the Organism, Mycobacterium abscessus, n. sp.* Journal of Investigative Dermatology, 1953. **20**(2): p. 133-169.
18. Maurer, F.P., et al., *Lack of antimicrobial bactericidal activity in Mycobacterium abscessus.* Antimicrobial agents and chemotherapy, 2014. **58**(7): p. 3828-3836.
19. Ferro, B.E., et al., *Failure of the amikacin, cefoxitin, and clarithromycin combination regimen for treating pulmonary Mycobacterium abscessus infection.* Antimicrobial Agents and Chemotherapy, 2016. **60**(10): p. 6374-6376.
20. Sanguinetti, M., et al., *Fatal pulmonary infection due to multidrug-resistant Mycobacterium abscessus in a patient with cystic fibrosis.* Journal of clinical microbiology, 2001. **39**(2): p. 816-819.
21. Roux, A.-L., et al., *The distinct fate of smooth and rough Mycobacterium abscessus variants inside macrophages.* Open biology, 2016. **6**(11): p. 160185.
22. Howard, S.T., et al., *Spontaneous reversion of Mycobacterium abscessus from a smooth to a rough morphotype is associated with reduced expression of glycopeptidolipid and reacquisition of an invasive phenotype.* Microbiology, 2006. **152**(6): p. 1581-1590.
23. Jo¨nsson, B.E., et al., *Molecular epidemiology of Mycobacterium abscessus, with focus on cystic fibrosis.* Journal of clinical microbiology, 2007. **45**(5): p. 1497-1504.
24. Kumar, H., T. Kawai, and S. Akira, *Pathogen recognition by the innate immune system.* International reviews of immunology, 2011. **30**(1): p. 16-34.
25. Weiss, G. and U.E. Schaible, *Macrophage defense mechanisms against intracellular bacteria.* Immunological reviews, 2015. **264**(1): p. 182-203.
26. Dubé, J.-Y., et al., *Underwhelming or misunderstood? Genetic variability of pattern recognition receptors in immune responses and resistance to Mycobacterium tuberculosis.* Frontiers in Immunology, 2021. **12**: p. 714808.
27. Shin, D.M., et al., *Mycobacterium abscessus activates the macrophage innate immune response via a physical and functional interaction between TLR2 and dectin-1.* Cellular microbiology, 2008. **10**(8): p. 1608-1621.
28. Ashida, H., et al., *Cell death and infection: a double-edged sword for host and pathogen survival.* Journal of Cell Biology, 2011. **195**(6): p. 931-942.
29. Häcker, G., *Apoptosis in infection.* Microbes and infection, 2018. **20**(9-10): p. 552-559.

30. Divangahi, M., S.M. Behar, and H. Remold, *Dying to live: how the death modality of the infected macrophage affects immunity to tuberculosis.* The new paradigm of immunity to tuberculosis, 2013: p. 103-120.
31. Lamkanfi, M. and V.M. Dixit, *Manipulation of host cell death pathways during microbial infections.* Cell host & microbe, 2010. **8**(1): p. 44-54.
32. Lee, J., et al., *Mycobacterium tuberculosis induces an atypical cell death mode to escape from infected macrophages.* PLoS One, 2011. **6**(3): p. e18367.
33. Amaral, E.P., et al., *A major role for ferroptosis in Mycobacterium tuberculosis–induced cell death and tissue necrosis.* Journal of Experimental Medicine, 2019. **216**(3): p. 556-570.
34. Dixon, S.J., et al., *Ferroptosis: an iron-dependent form of nonapoptotic cell death.* cell, 2012. **149**(5): p. 1060-1072.
35. Chung, J., D.J. Haile, and M. Wessling-Resnick, *Copper-induced ferroportin-1 expression in J774 macrophages is associated with increased iron efflux.* Proceedings of the National Academy of Sciences, 2004. **101**(9): p. 2700-2705.
36. Ratledge, C., *Iron, mycobacteria and tuberculosis.* Tuberculosis (Edinb), 2004. **84**(1-2): p. 110-30.
37. Catherinot, E., et al., *Hypervirulence of a rough variant of the Mycobacterium abscessus type strain.* Infection and immunity, 2007. **75**(2): p. 1055-1058.
38. Catherinot, E., et al., *Acute respiratory failure involving an R variant of Mycobacterium abscessus.* Journal of clinical microbiology, 2009. **47**(1): p. 271-274.
39. Cullen, A.R., et al., *Mycobacterium abscessus infection in cystic fibrosis: colonization or infection?* American journal of respiratory and critical care medicine, 2000. **161**(2): p. 641-645.
40. Je, S., et al., *Mycobacterium massiliense induces macrophage extracellular traps with facilitating bacterial growth.* PLoS One, 2016. **11**(5): p. e0155685.
41. Whang, J., et al., *Mycobacterium abscessus glycopeptidolipids inhibit macrophage apoptosis and bacterial spreading by targeting mitochondrial cyclophilin D.* Cell Death & Disease, 2017. **8**(8): p. e3012-e3012.
42. Kim, B.-R., et al., *Mycobacterium abscessus infection leads to enhanced production of type 1 interferon and NLRP3 inflammasome activation in murine macrophages via mitochondrial oxidative stress.* PLoS pathogens, 2020. **16**(3): p. e1008294.
43. Dixon, S.J. and B.R. Stockwell, *The role of iron and reactive oxygen species in cell death.* Nature chemical biology, 2014. **10**(1): p. 9-17.
44. Xu, G., et al., *Serum lipocalin-2 is a potential biomarker for the clinical diagnosis of nonalcoholic steatohepatitis.* Clinical and Molecular Hepatology, 2021. **27**(2): p. 329.
45. Roux, A.L., et al., *Overexpression of proinflammatory TLR-2-signalling lipoproteins in hypervirulent mycobacterial variants.* Cellular microbiology, 2011. **13**(5): p. 692-704.

46. Rhoades, E.R., et al., *Mycobacterium abscessus glycopeptidolipids mask underlying cell wall phosphatidyl-myo-inositol mannosides blocking induction of human macrophage TNF-α by preventing interaction with TLR2.* The Journal of Immunology, 2009. **183**(3): p. 1997-2007.
47. Bernut, A., et al., *Mycobacterium abscessus cording prevents phagocytosis and promotes abscess formation.* Proceedings of the National Academy of Sciences, 2014. **111**(10): p. E943-E952.
48. Wang, Y., et al., *The double-edged roles of ROS in cancer prevention and therapy.* Theranostics, 2021. **11**(10): p. 4839.
49. Zhao, R.Z., et al., *Mitochondrial electron transport chain, ROS generation and uncoupling.* International journal of molecular medicine, 2019. **44**(1): p. 3-15.
50. Nolfi-Donegan, D., A. Braganza, and S. Shiva, *Mitochondrial electron transport chain: Oxidative phosphorylation, oxidant production, and methods of measurement.* Redox biology, 2020. **37**: p. 101674.
51. Caverly, L.J., et al., *Mycobacterium abscessus morphotype comparison in a murine model.* PloS one, 2015. **10**(2): p. e0117657.
52. Fleury, C., B. Mignotte, and J.-L. Vayssière, *Mitochondrial reactive oxygen species and apoptosis*. 2001.
53. Chen, Z., X. Liu, and S. Ma, *The roles of mitochondria in autophagic cell death.* Cancer Biotherapy and Radiopharmaceuticals, 2016. **31**(8): p. 269-276.
54. Oh, S.-J., et al., *Mitochondrial event as an ultimate step in ferroptosis.* Cell Death Discovery, 2022. **8**(1): p. 414.
55. Indran, I.R., et al., *Recent advances in apoptosis, mitochondria and drug resistance in cancer cells.* Biochimica et Biophysica Acta (BBA)-Bioenergetics, 2011. **1807**(6): p. 735-745.
56. Bussi, C., et al., *Mycobacterium tuberculosis modulates mitochondrial function in human macrophages*. 2020, Eur Respiratory Soc.
57. Pagán, A.J., et al., *mTOR-regulated mitochondrial metabolism limits mycobacterium-induced cytotoxicity.* Cell, 2022. **185**(20): p. 3720-3738. e13.
58. Mohareer, K., et al., *Mycobacterial control of host mitochondria: bioenergetic and metabolic changes shaping cell fate and infection outcome.* Frontiers in Cellular and Infection Microbiology, 2020. **10**: p. 457.
59. Looney, M.M., et al., *Mycobacterium tuberculosis infection drives mitochondria-biased dysregulation of host transfer RNA-derived fragments.* The Journal of infectious diseases, 2021. **223**(10): p. 1796-1805.
60. Sohn, H., et al., *Targeting of Mycobacterium tuberculosis heparin-binding hemagglutinin to mitochondria in macrophages.* PLoS pathogens, 2011. **7**(12): p. e1002435.
61. Gutiérrez, A.V., et al., *Glycopeptidolipids, a double-edged sword of the Mycobacterium abscessus complex.* Frontiers in microbiology, 2018. **9**: p. 1145.

62. Chandra, P., S.J. Grigsby, and J.A. Philips, *Immune evasion and provocation by Mycobacterium tuberculosis.* Nature Reviews Microbiology, 2022. **20**(12): p. 750-766.
63. Mahamed, D., et al., *Intracellular growth of Mycobacterium tuberculosis after macrophage cell death leads to serial killing of host cells.* Elife, 2017. **6**: p. e22028.
64. George, K.M., et al., *A Mycobacterium ulcerans toxin, mycolactone, causes apoptosis in guinea pig ulcers and tissue culture cells.* Infection and immunity, 2000. **68**(2): p. 877-883.
65. Aguiló, N., et al., *ESX-1-induced apoptosis during mycobacterial infection: to be or not to be, that is the question.* Frontiers in cellular and infection microbiology, 2013. **3**: p. 88.
66. Guinn, K.M., et al., *Individual RD1-region genes are required for export of ESAT-6/CFP-10 and for virulence of Mycobacterium tuberculosis.* Molecular microbiology, 2004. **51**(2): p. 359-370.
67. Gao, L.Y., et al., *A mycobacterial virulence gene cluster extending RD1 is required for cytolysis, bacterial spreading and ESAT-6 secretion.* Molecular microbiology, 2004. **53**(6): p. 1677-1693.
68. Bryant, J.M., et al., *Emergence and spread of a human-transmissible multidrug-resistant nontuberculous mycobacterium.* Science, 2016. **354**(6313): p. 751-757.
69. Lopeman, R.C., et al., *Mycobacterium abscessus: environmental bacterium turned clinical nightmare.* Microorganisms, 2019. **7**(3): p. 90.
70. Lee, M.-R., et al., *Mycobacterium abscessus complex infections in humans.* Emerging infectious diseases, 2015. **21**(9): p. 1638.
71. Esther, C.R., Jr., et al., *Chronic Mycobacterium abscessus infection and lung function decline in cystic fibrosis.* J Cyst Fibros, 2010. **9**(2): p. 117-23.
72. Jarand, J., et al., *Clinical and microbiologic outcomes in patients receiving treatment for Mycobacterium abscessus pulmonary disease.* Clin Infect Dis, 2011. **52**(5): p. 565-71.
73. Nessar, R., et al., *Mycobacterium abscessus: a new antibiotic nightmare.* J Antimicrob Chemother, 2012. **67**(4): p. 810-8.
74. Kwak, N., et al., *M ycobacterium abscessus pulmonary disease: individual patient data meta-analysis.* Eur Respir J, 2019. **54**(1).
75. Taylor, J.L. and S.M. Palmer, *Mycobacterium abscessus chest wall and pulmonary infection in a cystic fibrosis lung transplant recipient.* J Heart Lung Transplant, 2006. **25**(8): p. 985-8.
76. Ruis, C., et al., *Dissemination of Mycobacterium abscessus via global transmission networks.* Nat Microbiol, 2021. **6**(10): p. 1279-1288.
77. Zumla, A., et al., *Host-directed therapies for infectious diseases: current status, recent progress, and future prospects.* The Lancet Infectious Diseases, 2016. **16**(4): p. e47-e63.
78. Kaufmann, S.H., et al., *Host-directed therapies for bacterial and viral infections.* Nature reviews Drug discovery, 2018. **17**(1): p. 35-56.
79. Palucci, I. and G. Delogu, *Host directed therapies for tuberculosis:*

futures strategies for an ancient disease. Chemotherapy, 2018. **63**(3): p. 172-180.
80. Kilinç, G., et al., *Host-directed therapy to combat mycobacterial infections.* Immunological reviews, 2021. **301**(1): p. 62-83.
81. Zhang, S., et al., *The pivotal role of pyruvate dehydrogenase kinases in metabolic flexibility.* Nutrition & metabolism, 2014. **11**(1): p. 1-9.
82. Stacpoole, P.W., *Therapeutic targeting of the pyruvate dehydrogenase complex/pyruvate dehydrogenase kinase (PDC/PDK) axis in cancer.* JNCI: Journal of the National Cancer Institute, 2017. **109**(11).
83. Jeoung, N.H., *Pyruvate dehydrogenase kinases: therapeutic targets for diabetes and cancers.* Diabetes & metabolism journal, 2015. **39**(3): p. 188-197.
84. Jung, G.-S., et al., *Pyruvate dehydrogenase kinase regulates hepatitis C virus replication.* Scientific Reports, 2016. **6**(1): p. 1-13.
85. van Doorn, C.L., et al., *Pyruvate Dehydrogenase Kinase Inhibitor Dichloroacetate Improves Host Control of Salmonella enterica Serovar Typhimurium Infection in Human Macrophages.* Frontiers in immunology, 2021: p. 3664.
86. Na, Y.R., et al., *Pyruvate dehydrogenase kinase is a negative regulator of interleukin-10 production in macrophages.* Journal of molecular cell biology, 2020. **12**(7): p. 543-555.
87. Na, Y.R., et al., *GM-CSF Induces Inflammatory Macrophages by Regulating Glycolysis and Lipid Metabolism.* J Immunol, 2016. **197**(10): p. 4101-4109.
88. Li, Y. and Y. Chen, *AMPK and autophagy.* Autophagy: Biology and Diseases, 2019: p. 85-108.
89. Herzig, S. and R.J. Shaw, *AMPK: guardian of metabolism and mitochondrial homeostasis.* Nature reviews Molecular cell biology, 2018. **19**(2): p. 121-135.
90. Gutierrez, M.G., et al., *Autophagy is a defense mechanism inhibiting BCG and Mycobacterium tuberculosis survival in infected macrophages.* Cell, 2004. **119**(6): p. 753-766.
91. Singh, S.B., et al., *Human IRGM induces autophagy to eliminate intracellular mycobacteria.* Science, 2006. **313**(5792): p. 1438-1441.
92. Rubinsztein, D.C., C.F. Bento, and V. Deretic, *Therapeutic targeting of autophagy in neurodegenerative and infectious diseases.* Journal of Experimental Medicine, 2015. **212**(7): p. 979-990.
93. Kim, Y.S., et al., *The peroxisome proliferator-activated receptor α-agonist gemfibrozil promotes defense against mycobacterium abscessus infections.* Cells, 2020. **9**(3): p. 648.
94. Park, C.R., et al., *Rufomycin Exhibits Dual Effects Against Mycobacterium abscessus Infection by Inducing Host Defense and Antimicrobial Activities.* Frontiers in microbiology, 2021: p. 2110.
95. Gleeson, L.E., et al., *Cutting edge: Mycobacterium tuberculosis induces aerobic glycolysis in human alveolar macrophages that is required for control of intracellular bacillary replication.* The Journal of Immunology, 2016. **196**(6): p. 2444-2449.

96. Hackett, E.E., et al., *Mycobacterium tuberculosis Limits Host Glycolysis and IL-1beta by Restriction of PFK-M via MicroRNA-21.* Cell Rep, 2020. **30**(1): p. 124-136 e4.
97. Wang, T., et al., *HIF1a-induced glycolysis metabolism is essential to the activation of inflammatory macrophages.* Mediators of inflammation, 2017. **2017**.
98. Palsson-McDermott, E.M., et al., *Pyruvate kinase M2 regulates Hif-1a activity and IL-1β induction and is a critical determinant of the warburg effect in LPS-activated macrophages.* Cell metabolism, 2015. **21**(1): p. 65-80.
99. Shi, L., et al., *Infection with Mycobacterium tuberculosis induces the Warburg effect in mouse lungs.* Scientific reports, 2015. **5**(1): p. 1-13.
100. Lachmandas, E., et al., *Rewiring cellular metabolism via the AKT/mTOR pathway contributes to host defence against Mycobacterium tuberculosis in human and murine cells.* European journal of immunology, 2016. **46**(11): p. 2574-2586.
101. Kelly, B. and L.A. O'neill, *Metabolic reprogramming in macrophages and dendritic cells in innate immunity.* Cell research, 2015. **25**(7): p. 771-784.
102. Mihaylova, M.M. and R.J. Shaw, *The AMPK signalling pathway coordinates cell growth, autophagy and metabolism.* Nature cell biology, 2011. **13**(9): p. 1016-1023.
103. Young, N.P., et al., *AMPK governs lineage specification through Tfeb-dependent regulation of lysosomes.* Genes & development, 2016. **30**(5): p. 535-552.
104. Gong, F., et al., *Dichloroacetate induces protective autophagy in LoVo cells: involvement of cathepsin D/thioredoxin-like protein 1 and Akt-mTOR-mediated signaling.* Cell death & disease, 2013. **4**(11): p. e913-e913.
105. Lin, G., et al., *Dichloroacetate induces autophagy in colorectal cancer cells and tumours.* British journal of cancer, 2014. **111**(2): p. 375-385.
106. Renna, M., et al., *Azithromycin blocks autophagy and may predispose cystic fibrosis patients to mycobacterial infection.* The Journal of clinical investigation, 2011. **121**(9).
107. Pohl, K., et al., *Mycobacterium abscessus clearance by neutrophils is independent of autophagy.* Infection and Immunity, 2020. **88**(8): p. e00024-20.
108. Falkinham III, J.O., *Challenges of NTM drug development.* Frontiers in microbiology, 2018. **9**: p. 1613.
109. Sethiya, J.P., et al., *MmpL3 inhibition: A new approach to treat nontuberculous mycobacterial infections.* International journal of molecular sciences, 2020. **21**(17): p. 6202.

국문초록

Mycobacteroides abscessus (*M. abscessus*)는 인간에게 폐렴을 유발하는 전염성 비결핵성 항산균 중 하나이며, 일차적인 항결핵약물 및 대부분의 항생제에 내재적이거나 유도적인 내성으로 인해 치료가 어려운 질환이다. 세포벽 표면 glycopeptidolipids (GPLs)를 가지고 있는 smooth 표현형인 *M. abscessus* (Ma^{Sm})에 비해 GPLs이 없는 rough 표현형인 *M. abscessus* (Ma^{Rg})더 심각하고 지속적인 감염과 관련되어 있으나, Ma^{Rg}의 병원성 메커니즘과 병원성 인자와의 관계는 여전히 불명확하다. 본 연구에서는 ferroptosis가 *M. abscessus* 감염에서 특히 Ma^{Rg}의 번식에 역할을 하는 것으로 나타나며, Ma^{Rg}의 외부 세포벽 지질인 phosphatidyl-myo-inositol mannoside-Franction 7(PIM-F7)이 ferroptosis를 유발하여 Ma^{Rg}의 병원성과 번식을 촉진한다는 것을 제시하였다. 이는 *M. abscessus*의 병원성 메커니즘에 대한 새로운 통찰력을 제공한다. 메커니즘적으로, PIM-F7이 Toll-like receptor 2 (TLR2) 의존적인 철 축적을 통해 미토콘드리아 ROS 생성과 상호작용하고, 이 상호작용이 지질 과산화를 활성화하고 ferroptosis를 유도하여 Ma^{Rg}의 병원성과 전파를 촉진한다는 것을 발견하였다. 이러한 결과들은 병원체 유발 ferroptosis의 분자 메커니즘에 대한 통찰력을 제공하며, *M. abscessus*-숙주 상호작용을 차단하여 철 축적 의존적인 ferroptosis를 대상으로 하는 Ma^{Rg} 치료법의 가능성을 제시하였다(제1장). 또한 세포

대사 증가와 선천성 매크로파지 면역 사이의 강력한 상호 작용을 입증하고 매크로파지 *Mycobacteroid massiliense* (*M. massiliense*)의 세포 내 복제가 숙주 pyruvate dehydrogenase kinase (PDK) 활성에 의존한다는 사실을 확인하였다. *M. massiliense* 감염은 매크로파지의 대사 변화를 유발하여 활성을 증가시키고 산화적 인산화를 감소시킨다. 그러나 PDK 억제제인 dichloroacetate(DCA)로 치료하면 감염된 대식세포에서 이러한 대사 전환이 역전되고 세포 내 복제가 제한된다. 메커니즘적으로 DCA는 AMP/ATP 비율을 증가시킴으로써 AMPK α1을 활성화하여 자가포식을 유도하고 식세포에서 박테리아 증식을 제한하는 것을 확인하였다. 이러한 결과는 DCA가 *M. massiliense* 감염을 제어하기 위한 숙주 지향적 치료의 타겟 약물이 될 수 있음을 시사한다(2장).

주요어: *Mycobacteroides abscessus*, 외부 세포벽 지질, 페롭토시스, 전파, DCA, 자가포식, 숙주 면역 방어

학 번: 2016-31941